Maria del Carmen Lavilla Gomez

Licenciada em Bioquímica

Synthesis and Characterization of pH Stimuli-Responsive Mesoporous Silica Nanoparticles

Dissertação para obtenção do Grau de Mestre em

Genética Molecular e Biomedicina

Orientador: José Paulo Farinha, Professor Doutor, IST-UL.

Co-orientador: Carlos Baleizão, Doutor, IST-UL.

Presidente: Prof. Doutora Paula Maria Theriaga Mendes Bernardo Gonçalves

Arguente: Prof. Doutor Frederico Castelo Ferreira

Vogal: Prof. Doutor José Paulo Sequeira Farinha

FACULDADE DE CIÊNCIAS E TECNOLOGIA
UNIVERSIDADE NOVA DE LISBOA

Dezembro 2016

UNIVERSIDADE NOVA DE LISBOA

FACULDADE DE CIÊNCIAS E TECNOLOGIA

DEPARTAMENTO DE CIÊNCIAS DA VIDA

Maria del Carmen Lavilla Gomez

Synthesis and Characterization of pH Stimuli-Responsive Mesoporous Silica Nanoparticles

Dissertação apresentada para a obtenção do Grau de Mestre em Genética Molecular e Biomedicina, pela Universidade Nova de Lisboa, Faculdade de Ciências e Tecnologia

Orientador:

Professor Doutor José Paulo Farinha

LISBOA

2016

Synthesis and Characterization of pH Stimuli-Responsive Mesoporous Silica Nanoparticles

Acknowledgements

First and foremost, I would like to express my heartfelt gratitude and indebtedness to my supervisor Prof. José Paulo Farinha for accepting me in his laboratory and for his valuable guidance, encouragement, patience, critical review and worthy suggestions for this project, without which this work would not have materialized. Likewise, I would like to thank my co-Supervisor, Dr. Carlos Baleizão for his moral support and valuable advice.

For all the trust, advice, orientation and support in the lab and in this last year I would like to express my appreciation to Carina Crucho. Her expertise and experience as well as her willingness to teach others have been of great value to my current knowledge. There will be no organic laboratory that does not remind me of her.

I would like to thank to all the members of this group and from the Centro de Química-Física Molecular, Instituto Superior Técnico for their constant guidance, encouragement, patience and help given when needed as well as for the good moments offered. Especially, to Ana Sofia, Elizabete, Ines and Tânia for the good moments in the office. Moreover, I would like to express my gratitude to Bruno, Gema, Laurinda, Ritu and Susana, with whom I have shared my scientific and personal doubts, for all they have done for me. For all the patience, help and for the countless coffees shared I will never forget Ana Catarina, Filipa and Tiago.

Also, I could not forget Catarina, Cascão, Rita and Tiago for all the good moments, talks and laughs during the college. They have been always a constant encouragement for me in thick and thin. I am overwhelmed that life has enabled our paths to cross, their never ending support and advice brought out the best of me. I would also like to thank to my flat mates for all the great time together, for taking care of me and for reminding me that there is life outside from work.

Six years ago I undertook a knowledge adventure, it was not an easy pathway, and I could not be here without the support and trust of my loving parents and brother. I will always be grateful to them for the way they raised me, the moral values that they have taught me and for the way they always presented themselves available for any problem I had. To them and to my good friends that had given me the strength to never stop walking, I will always be grateful.

Finally, I could not forget to mention my sister Bárbara, that even if she left us a long time ago, she always had been next to me to remind me who I am and where I want to go. Because, life is too short for not being who you are and for not doing what you love.

Resumo

No campo da bionanotecnologia tem sido crescente o interesse em desenvolver dispositivos médicos pelas suas possíveis aplicações na monitorização de doenças, terapia e diagnóstico. Nanopartículas mesoporosas de sílica (MSNs) têm sido usadas em sistemas de libertação de fármacos como veículos de transporte pela sua excelente biocompatibilidade, pela uniformidade e adaptabilidade do tamanho dos poros e pela grande diversidade de funcionalização da superfície. O revestimento das MSNs com um polímero *stimuli-responsive* permite o controlo sobre a libertação de fármaco como resposta a uma condição fisiológica específica, e/ou como resposta a um estímulo externo. Desta forma, é possível proteger o agente terapêutico de ser metabolizado pelo organismo e aumentar a sua eficiência e biodisponibilidade no sangue, ao mesmo tempo que são reduzidos os seus efeitos adversos.

O objectivo deste trabalho consistiu em desenvolver MSN híbridas núcleo-coroa, contendo um composto fluorescente no núcleo, e com uma coroa polimérica que apresenta uma mudança conformacional entre expandido e colapsado induzida por alteração do pH, combinando num único vector capacidades terapêuticas e de diagnóstico. A coroa polimérica foi preparada por polimerização RAFT (Reversible Addition-Fragmentation Chain Transfer) de forma a obter uma coroa homogénea e bem definida.

A distribuição de tamanhos do sistema híbrido foi determinada por microscopia de transmissão electrónica (TEM) e por dispersão de luz dinâmica (DLS), tendo sido obtidos diâmetros de aproximadamente 150 nm. A caracterização da coroa polimérica foi realizada por espectroscopia de Ressonância Magnética Nuclear de protão (^{1}H NMR), Infravermelho (FT-IR) e mobilidade electroforética (potencial zeta). A resposta ao pH foi comprovada por Potencial-Zeta tendo sido estimado o pH ao qual ocorre a transição conformacional de aproximadamente 6.2 – 6.5.

As nanopartículas híbridas indicam ser biocompatíveis após ensaios em células de adenocarcinoma pulmonar humano (MCF-7), em que para uma concentração de 125 µg/mL a viabilidade celular é superior a 70 %.

Palavras Chave: coroa polimérica, nanopartículas mesoporosas de sílica, nanopartículas híbridas, RAFT, resposta ao pH.

Abstract

In the field of bionanotechnology, the interest in the development of healthcare devices has increased due to their applications on diagnostics and therapeutics. Mesoporous silica nanoparticles (MSNs) have been used in drug delivery systems (DDSs) as nanocarriers due their excellent biocompatibility, high surface areas, large pore volumes, high payload, uniform and tunable pore sizes, and versatile of surface functionalization. The incorporation of a stimuli-responsive polymeric shell allows the drug release control response through a disease-specific physiological conditions, and/or from external applied *stimuli*. Additionally, it will protect the therapeutic molecules from physiological metabolization and enhance its efficiency and bioavailability in the bloodstream, as well as reduce the side effects. The goal of this work was to prepare a fluorescent core-shell MSNs, coated with a pH-responsive polymeric shell, combining diagnostic and therapeutic properties in a single vector. Reversible Addition-Fragmentation Chain Transfer (RAFT) polymerization was used to obtain a homogeneous polymeric shell with a well-defined structure.

The hybrid nanoparticles were characterized by Transmission Electronic Microscopy (TEM) and Dynamic Light Scattering (DLS), allowing diameters around 150 nm. The polymeric shell was characterized by Proton Nuclear Magnetic Resonance spectroscopy (^{1}H NMR), Fourier Transform Infrared Spectroscopy (FT-IR) and electrophoretic mobility (ζ-potential). The pH responsive behavior was proven by ζ-Potential with an estimated conformational transition at pH between 6.2 – 6.5.

The hybrid nanoparticles indicate being biocompatible tested by cell viability assays in human breast adenocarcinoma (MCF-7), which showed that for a concentration of 125 µg/mL the cell viability is over 70 %.

Key-Words: hybrid nanoparticles, mesoporous silica nanoparticles, RAFT, pH-response, polymeric shell.

General Contents

Figure Index

Scheme Index

Table Index

Abbreviation List

Abs	Absorbance
AIBN	2,2′-Azobis(2-methylpropionitrile)
APTES	(3-Aminopropyl) triethoxysilane
ATRP	Atom Transfer Radical Polymerization
CMC	Critical Micellar Concentration
CP	Chain Polymerization
CRP	Controlled Radical Polymerization
CSIRO	Commonwealth Scientific and Industrial Research Organisation
CTA	Chain Transfer Agent
CTAB	Hexadecyltrimethylammonium Bromide
D_H	Hydrodynamic Diameter
DI	Deionized
DLS	Dynamic Light Scattering
DPAEM	2-(diisopropylamino)ethyl methacrylate
D_{TEM}	Diameter obtained by Transmission Electronic Microscopy
EDC	N-(3-dimethylaminopropyl) -N′-ethylcarbodiimide
FT-IR	Fourier Transform Infrared
H^1 NMR	Pronton Nuclear Magnetic Resonance
MCM-41	Mobil Composition of Matter Number 41
MSN	Mesoporous Silica Nanoparticles
MSN.APTES	Mesoporous Silica Nanoparticles Surface Modified with APTES
MSN.RAFT	MSN.APTES linked to RAFT Agent
MSN.P(DPAEM)	MSN coated with DPAEM polymer obtained by grafting from

MSN.G P(DPAEM)	MSN coated with DPAEM polymer obtained by grafting to
MW	Molecular Weight
NMP	Nitroxide-Mediated Polymerization
NNI	National Nanotechnology Initiative
P(DPAEM)	Poly (2-(diisopropylamino)ethyl methacrylate)
PBS	Phosphate Buffered Saline
PDI	Perylenediimide
IEP	Isoelectric Point
pK_a	Acid Dissociation Constant
RAFT	Reversible Addition-Fragmentation Chain Transfer
RP	Radical Polymerization
TEM	Transmission Electronic Microscopy
TEOS	Tetraethyl Orthosilicate
TFA	Tetrahydrofuran
THF	Tetrahydrofuran
UV	Ultraviolet
ZP	ζ-Potential

Unit List

Da	Dalton
Eq	Equivalent
g; mg	Grams; milligrams (10^{-3} g)
h; min; s	hours; minutes; seconds
K	Kelvin
kV; mV	Kilovolts (10^{3} V); millivolts (10^{-3} V)
L; mL	Litre; millilitre (10^{-3} L)
M	Molar
m, cm, µm, nm	meter; centimeter (10^{-2} m); micrometer (10^{-6} m); nanometer (10^{-9} m)
MHz	Megahertz
mol; mmol	Mol; millimol (10^{-3} mol)
MΩ	Megaohm
ppm	Parts per million
rpm	Rotations per minute
x g	Times gravity

Symbol List

[AIBN]	AIBN concentration
[APTES]	APTES concentration
δ	Bending vibration
c	Concentration
ρ	Conversion
$\mathbf{M_{CTA}}$	CTA MW
$\mathbf{[CTA]_0}$	Initial CTA concentration
$\mathbf{[M]_0}$	Initial Monomer concentration
l	Length
ε	Molar Absorptivity
$\mathbf{M_{mon}}$	Monomer MW
[NaOH]	NaOH concentration
$\mathbf{M_n}$	Polymer MW
N	Stretching vibration
Λ	Wavelength

1. Introduction

The nanotechnology concept appears in 1959 with the physicist Richard Feynman in a lecture entitled “There’s Plenty of Room at the Bottom”, where he refers for the first time the possibility of handling materials in a nanoscale by using atomic and molecular units (Feynman, 1959; Goodsell, 2004; “National Nanotechnology Initiative”, 2015; Singh, 2010). Nowadays, nanotechnology is known as a multidisciplinary scientific field that involves the manipulation of matter to design and engineer devices at the nanoscale, according to the National Nanotechnology Initiative (NNI) between 1 and 100 nm range at least in one dimension (Ferrari, 2005; Jain, 2005; “National Nanotechnology Initiative”, 2015). The interest in those materials lies in their great potential applications in several disciplines due to their unique physical and chemical properties derived from their nano size (Ferrari, 2005; Jain, 2005; Mousa *et al.*, 2011; Singh, 2010).

In bio-nanotechnology, the development of healthcare devices has a great impact for its applications in diagnostics and therapeutics, by mimicking the “magic bullet concept”, proposed by Paul Ehrlich (Strebhardt *et al.*, 2008; Li *et al.*, 2012). This idea arises from the concern about low specificity and effectiveness due to the difficulties displayed by drugs in order to overcome the biological hurdles until reaching their target. Nevertheless, it is possible to overcome those pharmacokinetic and pharmacodynamics issues with selective and effective delivery systems by using nanocarriers, enhancing the efficiency and reducing the side effects (Argyo *et al.*, 2013; Cuenca *et al.*, 2006; Ferrari, 2005; Jain, 2005; Li, 2012; Mousa *et al.*, 2011; Singh, 2010; Tan *et al.*, 2004). Besides avoiding adverse side effects and increasing selectivity and specificity, drug delivery systems (DDS) have a great potential for personalized medicine on behalf of eradicating complex diseases, such as cancer, by integrating on the same dispositive detection, treatment, and monitoring of the disease in real time. These bionanotechnological devices are meant to replace invasive conventional methods used to track and treat diseases (Ferrari, 2005; Mousa *et al.*, 2011; Singh, 2010).

Several nanocarriers (Figure 1.1) have been developed in the field of nanomedicine classified as organic (liposomes, biodegradable polymers, dendrimers, carbon nanotubes, etc.), inorganic (quantum dots, inorganic nanoparticles, etc.) or hybrid (with two different compounds). These systems are able to improve the methods used for diagnostics and therapeutics by having in mind biocompatibility and biodegradability of the materials used in nanocarriers fabrication (Cuenca *et al.*, 2006; Mousa *et al.*, 2011; Singh, 2010).

Nanoparticles have shown a great potential in medicine not only due to its unique chemical and physical properties derived from their nano size, but also due to its maximum surface to volume ratio that allowing surface functionalization as well as the incorporation of a therapeutics load. All these features enable better access to the target as compared to conventional nanocarriers. Therefore, the use of nanoparticles as DDS improves tissue selectivity uptake and provides drugs protection against degradation (Li, 2012; Mousa *et al.*, 2011; Tan *et al.,* 2004).

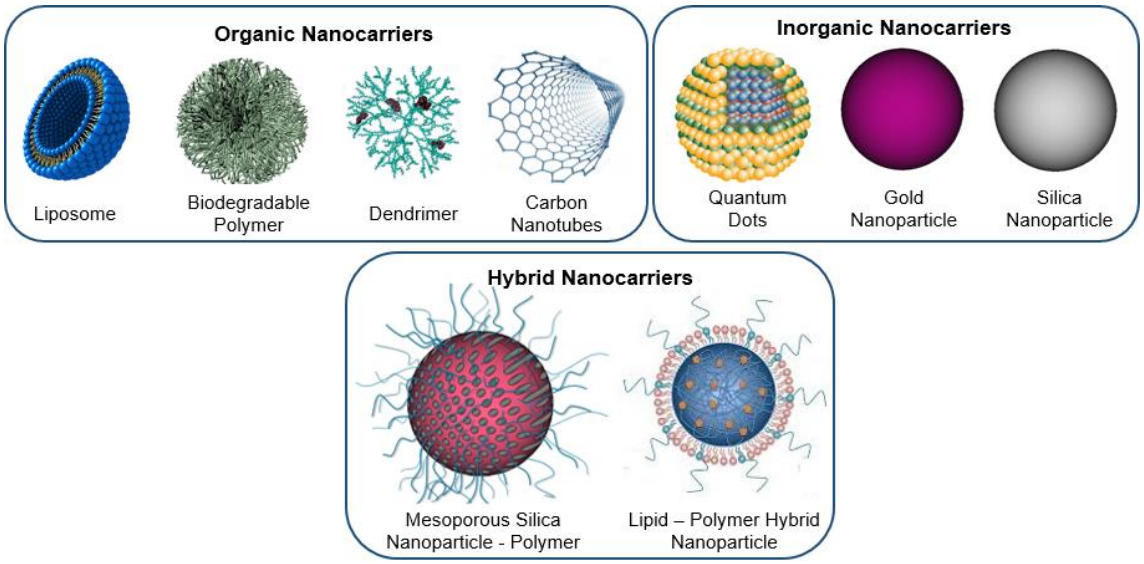

Figure 1.1. Examples of different organic, inorganic and hybrid nanocarriers.

1.1. Mesoporous Silica Nanoparticles

The importance of silica nanoparticles rises from its unique properties such as mechanical strength, permeability, thermal and chemical stability, low refractive index, high surface area as well as its versatile surface chemistry. The last two properties allow bioconjugation with other molecules through surface modification, either by the reaction the silanols groups (at the surface of the nanoparticle) or by adsorption on the surface. Apart from the previously mentioned characteristics, size, shape, and inner structure can be tuned accordingly to the desired application (Ahmadi *et al.*, 2014; Argyo *et al.*, 2013; Huh *et al.*, 2003; Li *et al.*, 2012; Schulz *et al.*, 2012; Slowing *et al.*, 2006; Trewyn *et al.*, 2007; Vallet-Regí, 2012; Wang *et al.*, 2009). This discovery was made by Mobil Oil Corporation in 1992 through the development of highly ordered mesoporous silica materials known as Mobil Composition of Matter Number 41 (MCM-41) (Argyo *et al.*, 2013; Trewyn *et al.*, 2007; Vallet-Regí, 2012). Those materials are characterized by uniform cylindrical pores with tuneable diameters (between 2 and 50 nm) which result in a large pore volume and high surface area (700–1500 m^2/g) and large pore volume (1 mL/g). All these features make them ideal materials for DDS, making possible to host several molecules inside the pores, regardless of their nature (Argyo *et al.*, 2013; Trewyn *et al.*, 2007; Vallet-Regí, 2012).

Mesoporous silica nanoparticles for DDs requires controlling the diameter of the nanoparticles, as well as the volume, shape and organization of the mesopores, depending on its application (Figure 1.2). These modifications can be performed by tuning different parameters, such as the template, temperature, pH, etc. (Argyo *et al.*, 2013; Trewyn *et al.*, 2007; Vallet-Regí, 2012).

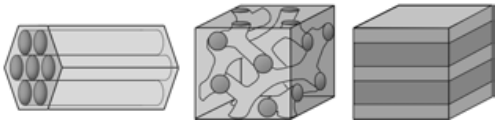

Figure 1.2. The different pore structure of mesoporous silica materials.

It is worth mentioning that the tridimensional network that constitutes these particles is formed by silanol groups (Si-OH) throughout the whole particle surface (including the surface of the pores) and by siloxane groups (≡Si-O-Si≡) inside the network, rendering these particles a hydrophilic behaviour (Ahmadi *et al.*, 2014; Tan *et al.,* 2004; Vallet-Regí, 2012).

The thermal and chemical stability, controllable morphology, easiness of synthesis and functionalization, low toxicity, biodegradability and biocompatibility, combined with high loading capacity, make these materials perfect candidates for application in therapy and diagnosis (theranostics) (Ahmadi *et al.*, 2014; Argyo *et al.*, 2013; Vallet-Regí, 2012). For particle sizes between 50-160 nm, the cellular uptake efficiency has been proven to supports, even more, the evidence of the capacity of these materials for the referred purposes (Zhu *et al.*, 2013).

1.2. Silica Nanoparticle Synthesis

The several methods that have been developed to obtain nanoparticles can be categorized into two main approaches: top-down and bottom-up. The top-down approach, also known as physical approach, is based on reducing the dimension of the original material by using physical techniques. On the other side, the bottom-up or chemical approach involves the decomposition of the precursor into atoms or molecules which nucleate and grow producing a colloid solution (Cunningham *et al.*, 2013; Chaudhuri *et al.*, 2011; Storhoff *et al.*, 1997).

The bottom-up approach is becoming widely used since this versatile technique allows the production of structures on a small-scale and complex architecture, never achieved before with the top-down approach. Moreover, unlike the top-down approach, such technique permits large scale and faster production without requiring expensive equipment. The most common methods based on bottom-up approach are: flame synthesis, reverse microemulsion, and sol-gel process (Chaudhuri *et al.*, 2011; Tan *et al.,* 2004).

1.2.1. Sol-Gel Synthesis

The sol-gel is the best technique to obtain more efficiently organized structures, control size distribution and morphology. It uses liquid solutions of synthetic raw materials with low viscosity, allowing high purity, great homogenization at the molecular level, and requires lower temperatures than other procedures, avoiding vaporization losses and phase transformations. The production of homogenous structures by controlling physical-chemical variability is the goal of the sol-gel processing in order to control the surface and interface characteristics of the material (Hench *et al.*, 1990; Soler-Illia *et al.*, 2011; Tang *et al.*, 2012).

The synthesis of silica nanoparticles is usually based on this procedure due to its ability to easily control particle size, size distribution, and morphology by simply monitoring the reaction parameters. The sol-gel synthesis can be performed using either acidic (hydrochloric acid, nitric acid, etc.) or basic conditions (sodium or ammonium hydroxide) to catalyse the hydrolysis of the silica precursor, yielding a colloidal solution (*sol*) constituted by silanol groups (Scheme 1.1 - A). Two types of silica precursors are usually used for silica nanoparticles synthesis: inorganic salts (sodium silicates) or metal alkoxides (tetra-alkyl oxide of silane). Afterwards, the condensation between the silanol groups (Scheme 1.1 - B) or between silanol groups and ethoxy groups (Scheme 1.1 - C) originates siloxane bridges (Si-O-Si) that establish the silica network (*gel*) (Green *et al.*, 2003).

A. Hydrolysis	≡ Si – OR + H_2O ↔≡ Si – OH + ROH
B. Alcohol condensation	≡ Si – OR + HO – Si ≡ ↔ ≡ Si – O – Si ≡ + ROH
C. Water condensation	≡ Si – OH + HO – Si ≡ ↔ ≡ Si – O – Si ≡ + H_2O

Scheme 1.1. General scheme for hydrolysis (A) and condensation (B) and (C) in sol-gel.

Great efforts have been made to synthesise monodispersed and well define size and shape silica nanoparticles for research applications, offering experimental and theoretical advantages by simplifying data analyses and understand physiochemical properties and physiopathological effects of those particles (Stöber *et al.*, 1968).

1.2.1.1. Stöber Method

A pioneering method for the synthesis of monodispersed spherical silica particles was reported for the first time by Stöber *et al.* This method allows a controlled synthesis, obtaining spherical silica nanoparticles by using aqueous alcohol solutions of silica alkoxides, such as tetraethyl orthosilicate (TEOS, see figure 1.3), as silica precursor and ammonia as basic catalyst, producing particles with diameter from 5 to 2000 nm. The silica particle size is a function of the initial concentration of water and ammonia, the type of silicon alkoxides and alcohol used and reactant temperature (Stöber *et al.*, 1968; Tan *et al.,* 2004)

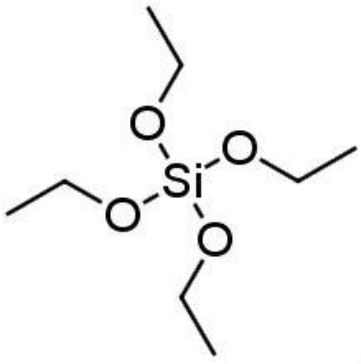

Figure 1.3. Chemical formula for silica precursor tetraethyl orthosilicate (TEOS).

As mentioned above, the mechanism of reactions to synthesize silica particles involves the hydrolysis and condensation of the silica precursor. In the Stöber method (Figure 1.4), an ethanol solution of TEOS hydrolises in the presence of ammonium hydroxide and water followed by the water and alcohol condensation between silanol groups or between silanol groups and ethoxy groups, respectively. This condensation gives place to siloxane bridges which establish the silica network (Green *et al.*, 2003).

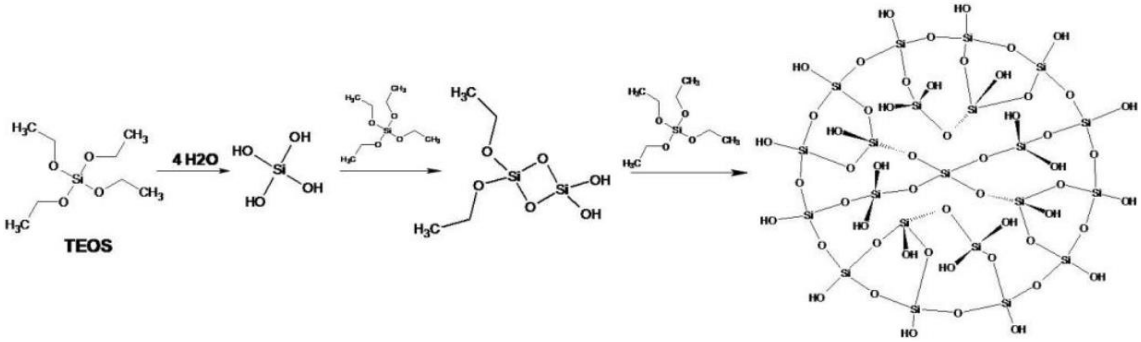

Figure 1.4. Hydrolysis and condensation reaction of TEOS described for Stöber method.

Indeed, the approaches used in the synthesis of monodispersed silica nanoparticles evolved from the Stöber method, by varying the silica alkoxides, the catalyst, temperature, etc.

1.2.1.2. Mesoporous Silica Nanoparticles Synthesis

In order to obtain monodispersed mesoporous silica nanoparticles (MSN) Grün *et al.* (Grün *et al.*, 2000) developed a synthesis procedure based on the Stöber method, by modifying the Stöber synthetic compositions through adding a cationic surfactant to the reaction mixture, reaching to submicrometer-scaled MCM-41 spherical particles (Huh *et al.*, 2003; Soler-Illia *et al.*, 2011; Trewyn *et al.*, 2007; Vallet-Regí, 2012).

Since then, the synthesis of mesoporous silica nanoparticles has been performed by using a surfactant in aqueous solution on order to take place the micelle's assembly (Figure 1.5 - A). When the surfactant concentration is higher than the critical micellar concentration (CMC), the surfactant molecules associate spontaneously, originating molecular aggregates, known as micelles, with several structures such as cylinders (Figure 1.5 - B). The formation and the dispersion of those structures in solution provide a template for the condensation of silica (Figure 1.5 - C). The addition of the catalyst and silica precursor to the solution originates the hydrolysis of the silica precursor and its condensation around the template (Figure 1.5 - D). Once removed the surfactant by calcination or acid extraction, the resultant particles are characterized by a hollow mesostructure (Figure 1.5 - E) (Argyo *et al.*, 2013; Huh *et al.*, 2003; Tang *et al.*, 2012; Trewyn *et al.*, 2007; Vallet-Regí, 2012).

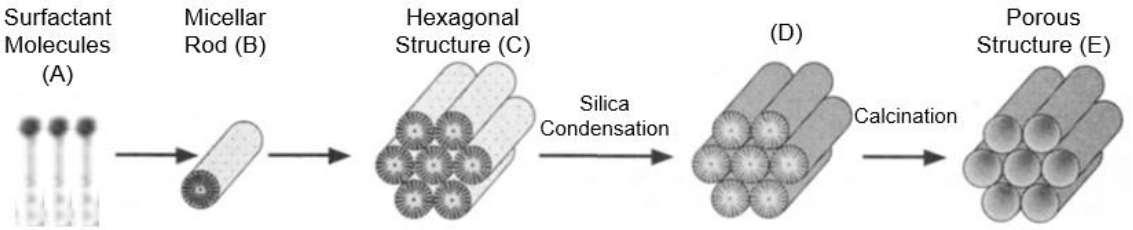

Figure 1.5. Illustration of mesoporous material formation (Adapted from Beck *et al.*, 1992).

Several synthetic methods have been reported in order to control nucleation and growth mechanism, to achieve an efficient synthesis of monodisperse MSN sizes and shape with well-defined mesostructures. The difference between the used methods lies on the variation of some parameters such as pH, temperature, solvents or catalysts and precursors. Yet, several compounds can be used as surfactant agents, all constituted by a hydrophobic head and a hydrophilic tail, exhibiting an amphiphilic behavior. Through the management of the surfactant structure, concentration or conditions of the solution it is possible to tune the shape and size of those nanoparticles' mesostructure (Argyo *et al.*, 2013; Soler-Illia *et al.*, 2011; Tang *et al.*, 2012; Trewyn *et al.*, 2007; Zhao *et al.*, 2009).

1.2.2. Surface Modification

The interest on MSNs applications in biomedicine, namely as drug delivery systems, drug targeting, gene transfection, tissue engineering or cell tracking, requires controlling the surface properties, improving drug uptake as well as enhancing its biocompatibility (Ahmadi *et al.*, 2014; Argyo *et al.*, 2013; Popat *et al.*, 2011; Schulz *et al.*, 2012; Slowing *et al.*, 2006; Tan *et al.,* 2004; Trewyn *et al.*, 2007; Vallet-Regí, 2012). In this way, it is possible to take advantage of its unique structure distinguished by high internal volume, narrow channels and a large surface area, characterized by the presence of silanol groups. This surface chemistry allows the functionalization with coupling groups (amine, carboxylic or thiol groups) providing active sites for attaching other molecules of interest (Figure 1.6) to MSN surface (Ahmadi *et al.*, 2014; Argyo *et al.*, 2013; Tan *et al.,* 2004; Trewyn *et al.*, 2007).

The functionalization of MSN's surface is attained using a modifying agent, usually an organo-substituted trialkoxysilane RSi(OR´)3. The hydrolyzable group (OR') reacts with the silanol groups located on the nanoparticle surface, anchoring the molecule covalently to the MSN surface. On the other hand, the R group brings new physicochemical properties to the MSN surface, providing it with new functionalities (Zou *et al.*, 2008). The modifying agent can be assembled to MSN surface by two different approaches, by co-condensation while the MSN is synthesized or by post-synthesis grafting. The co-condensation approach is characterized by a homogeneous distribution of the functional groups throughout the entire material, while with the grafting method approach the functional groups are mostly located on the external surface or at the proximities of the pore entrance (Argyo *et al.*, 2013; Huh *et al.*, 2003; Popat *et al.*, 2011; Stein *et al.*, 2000).

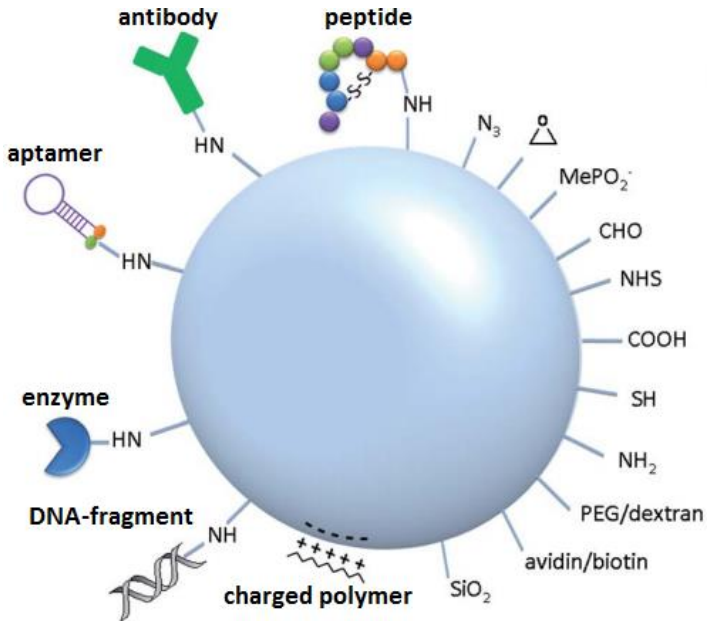

Figure 1.6. Schematic illustration of silica nanoparticles' surface functionalization with various functional groups and (bio)molecules (Adapted from Schulz *et al.*, 2012).

The grafting approach provides MSN with different regions of functionalization (Figure 1.7). The external surface (Figure 1.7 – a), as well as the pore entrance (Figure 1.7 – b), can be functionalized, while the surfactant is inside of the pores avoiding the internal functionalization, with moieties that improve biocompatibility, colloidal stability, and cellular uptake, allowing the detection and control drug release or even carry therapeutics. After the external surface modification, the surfactant can be removed, turning the pores available to host molecules or to internal functionalization (Figure 1.7 - c), increasing drug uptake by modifying interactions between the hosted molecules and the mesoporous silica nanoparticles medium (Argyo *et al.*, 2013; Slowing *et al.*, 2010; Vallet-Regí, 2012).

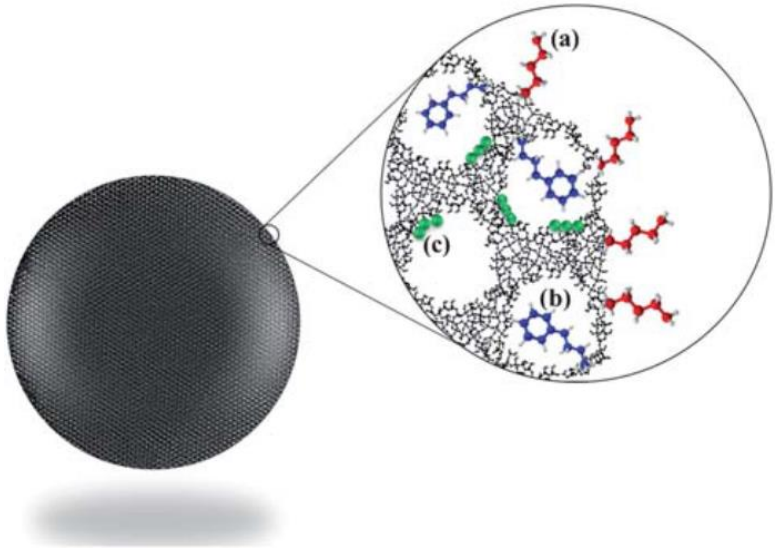

Figure 1.7. Functionalization in different regions of MSN: (a) at the external surface, (b) at the pore entrances, or (c) within the walls (Slowing *et al.*, 2010).

It is known that the uptake and release of drugs are dependent on the type of functional groups found at MSN surface and consequently to the of interaction between this groups and the drug molecules. Therefore, the aim of MSN's functionalization on biomedicine field is to ensure better drug delivery, higher adsorption of the drug as well as retain the drug release until it reaches the target, improving effectiveness and minimizing drug adverse effects. In addition, the versatility of the silica surface has been used to immobilize different functional groups as needed for biosensing, bioimaging applications and to improve cellular uptake (Ahmadi *et al.*, 2014; Argyo *et al.*, 2013; Natarajan *et al.*, 2014; Popat *et al.*, 2011; Slowing *et al.*,2006; Tan *et al.*, 2004; Trewyn *et al.*, 2007).

Amine functionalized mesoporous silica materials have been largely studied for its high adsorption capacity, turning it into an ideal drug delivery medium (Ahmadi *et al.*, 2014; Slowing *et al.*, 2010; Vallet-Regí, 2012). A good example of an amine modifying agent is (3-Aminopropyl) triethoxysilane (APTES), allowing the amine group to cover MSNs surface (Figure 1.8), allowing the subsequent drug loading or even the incorporation of other organic molecules, such as polymers (Ahmadi *et al.*, 2014).

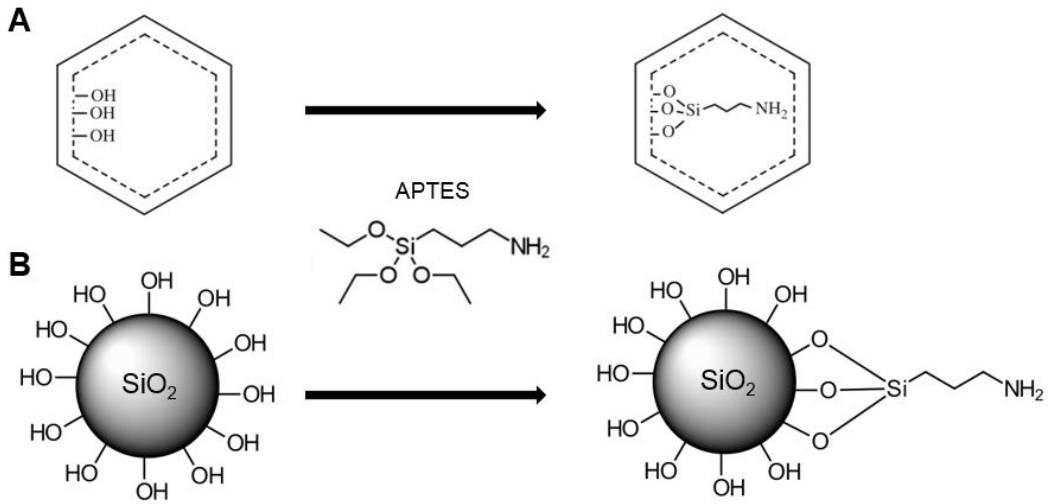

Figure 1.8. Schematic amine internal (A) and external (B) surface functionalization with APTES molecule.

1.3. Polymer-based Controlled Release Systems

Originally, polymers' application in the field of pharmacology intended to stabilize drugs and turn them soluble in physiological conditions (Kim *et al.*, 2009). Nevertheless, the development of new monomers and the better understanding of polymers' behavior have increased interest for its applications as controlled release systems due to its solubility, biocompatibility and capacity of modulating its structure as a response to determine metabolic states or physiological variations. Slight variations in the surrounding environment (pH, temperature, ionic strength, light and redox potential) cause extreme changes in the polymers' microstructure (Figure 1.9), modifying its physico-chemical properties in a reversible way (Bawa *et al.*, 2009; Cabane *et al.*, 2012; Gil *et al.*, 2004; Gupta *et al.*, 2002; Kim *et al.*, 2009; Schmaljohann, 2006; Singh, 2010).

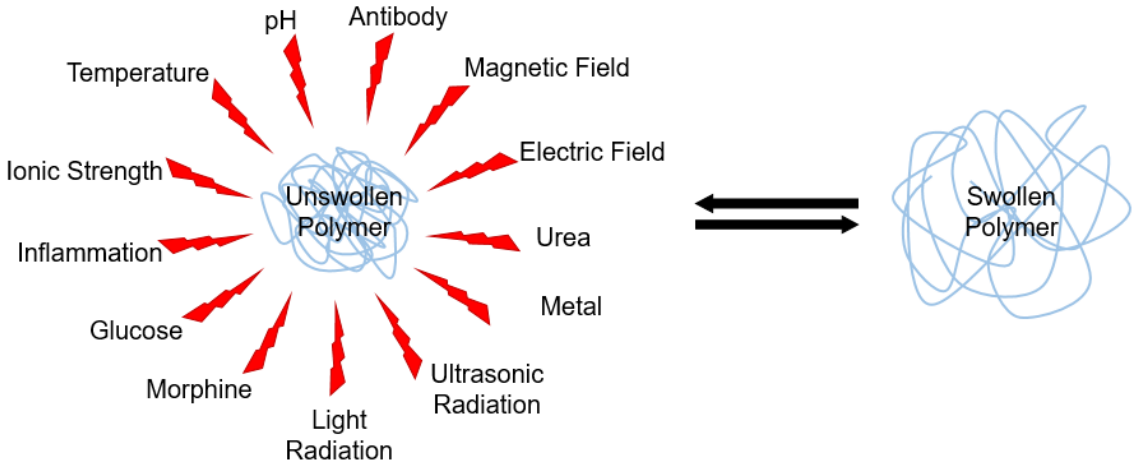

Figure 1.9. Stimuli that can induce polymeric conformational transitions.

Usually, polymer response is based on the formation/breaking of hydrogen bonds or/and electrostatic interactions or acid-base equilibria, leading to chain modifications on its size, secondary structure, solubility or intermolecular association (Cabane *et al.*, 2012; Dai *et al.*, 2008; Gupta *et al.*, 2002).

More specifically, the pH-responsive polymers' behavior is related with the ionizable groups present on its structure, which are able to accept and donate protons in response to pH environmental changes. When a specific pH (pK_a) is achieved, a dramatic transformation of the net charge occurs which causes a change of the hydrodynamic volume of the polymer chains. The osmotic pressure exerted by mobile counter ions that neutralize the network charges is responsible for the transition from collapsed to the expanded structure (Bawa *et al.*, 2009; Cabane *et al.*, 2012; Dai *et al.*, 2008; Gil *et al.*, 2004; Gupta *et al.*, 2002; Huh *et al.*, 2012; Schmaljohann, 2006).

There are four main types of pH-responsive polymers (Gil *et al.*, 2004):

A) Polyacids: their carboxylic pendant groups accept protons at low pH and release them at high pH. Therefore, they are converted into polyelectrolytes at high pH with electrostatic repulsion forces between the molecular chains. At that pH, a transition from hydrophilic (swollen) polymers into hydrophobic (unswollen) polymers occurs.
B) Polybases: The amine groups in their side chains are responsible for its sensitive pH response, which accept protons under acidic condition and loose them under basic condition.
C) pH -responsive degradable polymers: under specific pH (normally mildly acidic conditions) show fast degradation kinetics, while they are stable at physiological pH.
D) Biopolymers and artificial polypeptides: weakly ionizable polysaccharides, such as alginate and chitosan, show pH-responsive phase transition.

The critical pH (pK_a) where reversible conformation changes happen can be adjusted depending on polymer application, by the incorporation of a hydrophobic moiety into the polymer backbone (Bawa *et al.*, 2009; Gil *et al.*, 2004).

The use of these polymers as drug delivery systems increases drug efficiency since they are released in specific conditions enhancing the therapeutic effect. Furthermore, as mentioned before, the use of polymers improves the solubility and biocompatibility of the drug or the material inside its structure (Cabane *et al.*, 2012; Gupta *et al.*, 2002; Kim *et al.*, 2009).

Regarding biomedical applications, pH is an important environmental parameter, since pH changes occur in many specific or pathological compartments. More precisely, extracellular tumour tissue has shown a pH decrease (6.5 ~ 7.2) compared with healthy tissue. This enables the possibility to develop smart polymeric devices to carry anti-cancer treatment which respond to acidic conditions that characterize the tumour tissue (Bawa *et al.*, 2009; Cabane *et al.*, 2012; Dai *et al.*, 2008; Huh *et al.*, 2012; Kim *et al.*, 2009).

1.4. Hybrid Nanoparticles

Despite the fact that nanoparticles have been frequently used in the field of biomedicine through many years, they present some restrictions that can be overcome through the conjugation with another type of material (hybrid nanoparticles). Core-shell nanoparticles have been extensively studied due to their wide range of possible combinations (inorganic – inorganic, inorganic – organic, organic – inorganic and organic – organic) that yield hybrid materials with improved properties (Singh *et al.*, 2011).

As mentioned before, mesoporous silica nanoparticles exhibit some interesting properties regarding its application in biomedicine (See 1.1). However, the hydrophilic groups (silanol groups) located on the silica surface interact with cell membranes and promote reaction between particles through hydrogen bonds, inducing aggregation and disturbing nanoparticles' physicochemical properties behavior (Singh *et al.*, 2011). It is possible to overcome this pitfall by coating silica with a polymer, bringing not only the needed stability as well as improving biocompatibility and some other properties very useful for the biomedical applications (Argyo *et al.*, 2013; Liu *et al.*, 2009; Singh *et al.*, 2011; Zhao *et al.*, 2009).

Hybrid nanoparticles composed by silica-polymer core-shell are hard to obtain, due to the incompatibility between inorganic-organic materials. Usually, the synthesis of these hybrid nanoparticles is assisted by functionalization of silica surface (as described on 1.2.2), increasing compatibility as well as interactions between the two phases (Santiago *et al.*, 2015; Singh *et al.*, 2011).

Core-shell mesoporous silica nanoparticles coated with a polymer (Figure 1.10) have a great potential as drug delivery systems by combining drug hosting inside mesoporous silica structure with simultaneous higher biocompatibility, system stability and control the drug release (Chaudhuri *et al.*, 2011; Liu *et al.*, 2009; Santiago *et al.*, 2015; Singh *et al.*, 2011; Wang *et al.*, 2009).

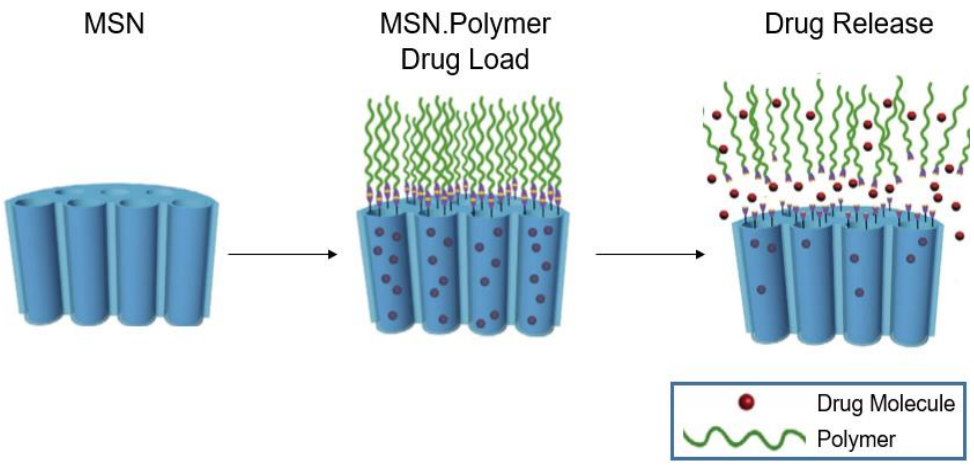

Figure 1.10. Adaptation of the schematic illustration of drug loading and release by core-shell mesoporous silica nanoparticle coated with a polymer (Adapted from Wang *et al.*, 2009).

1.5. Control Radical Polymerization

In the last two decades, great efforts have been made in order to obtain (co)polymers with well-defined weight and low polydispersity, as the polymers obtained by ionic chain polymerization, in relatively simple conditions that radical polymerization approach offers. Controlled Radical Polymerization (CRP) rises as the ideal approach to obtain polymers with a controlled structure in quite simple conditions by using the intermittent formation of active propagation species (Favier *et al.*, 2006; Gaynor *et al.*, 1994; Matyjaszewski, 1996; Odian, 2004; Vega-Rios *et al.*, 2011).

There are three main CRP techniques, namely atom transfer radical polymerization (ATRP), nitroxide-mediated polymerization (NMP) and reversible addition-fragmentation chain transfer (RAFT) (Moad *et al.*, 2005; Odian, 2004).

Reversible addition fragmentation chain transfer (RAFT) polymerization was first reported by CSIRO group in 1998 and it has been shown to be a highly effective and versatile method of controlled radical polymerization. Unlike other CRP, this technique is able to induce living behavior on a wide range of monomers in the same conditions as used in radical polymerization reaction (initiators, solvents, and reaction temperature) by adding an appropriate RAFT agent, leading to the synthesis of several polymers with a controlled MW and well-defined structure (Favier *et al.*, 2006; Moad *et al.*, 1998; Odian, 2004; Vega-Rios *et al.*, 2011).

This method provides *living* characteristics to radical polymerization through a reversible addition-fragmentation reaction mediated by chain transfer agents (CTAs), as thiocarbonylthio groups (S=C-S). CTAs, unlike radical polymerization, are capable of reversibly deactivate propagation radicals, maintaining the majority of the living chain in dormant form, providing living character to this kind of reaction. It is important to achieve the right conditions to support a fast equilibrium between the dormant polymer chain and the propagating radicals (Favier *et al.*, 2006; Moad *et al.*, 1998; Moad *et al.*, 2005; Odian, 2004; Vega-Rios *et al.*, 2011).

The importance of the living character of RAFT technique lies in the slight polydispersity between polymers obtained, the linear MW conversion profile, the MW predictability (Equation 1.1) and the capacity of producing blocks or higher MW polymers merely by adding more monomer (Favier *et al.*, 2006; Moad *et al.*, 1998; Odian, 2004; Vega-Rios *et al.*, 2011).

$$M_n \cong \frac{[M]_0 \times M_{mon} \times \rho}{[CTA]_0} + M_{CTA} \qquad (1.1)$$

Where $[M]_0$ is the initial monomer concentration, M_{mon} is the molecular weight of the monomer, ρ is the conversion, M_{CTA} is the molecular weight of the CTA, and $[CTA]_0$ is the initial concentration of the CTA (Vega-Rios *et al.*, 2011).

According to the monomers, as well as the conditions used in the polymerization, it is important to choose the right CTA to obtain the desired polymeric architecture. The CTA molecular structure is composed by a trithiocarbonate and dithioester (figure 1.11), providing specific characteristics to the CTA agent and controlling reaction kinetics. Free radical leaving group (R) must be able to reinitiate polymerization and the bond between R and S should be weak. The rate of radical addition and fragmentation depends on C=S reactive bond that is controlled by the Z group. Since Sigma-Aldrich started selling different CTAs, research on this field has increased significantly (Favier *et al.*, 2006; Moad *et al.*, 1998; Odian, 2004; Vega-Rios *et al.*, 2011).

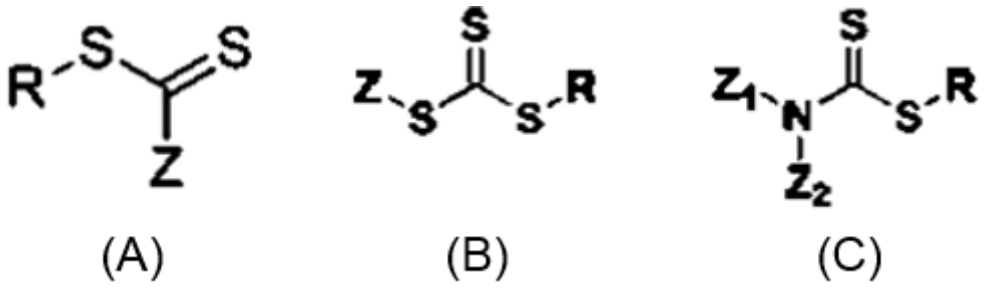

Figure 1.11. General structure of RAFT agent (A), trithiocarbonate (B) and dithioester (C).

This reaction is characterized by three events: initiation, propagation, and termination. The initiator 2,2′-Azobis(2-methylpropionitrile) (AIBN) is highly used in RAFT polymerization, being decomposed by UV irradiation or thermally, giving rise to a nitrogen molecule and two free radicals (2R*) (figure 1.12) (Moad *et al.*, 2005).

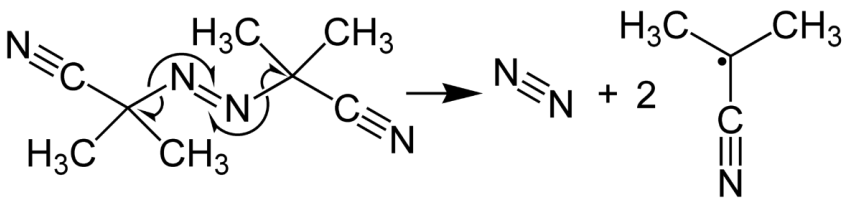

Figure 1.12. 2,2′-Azobis(2-methylpropionitrile) AIBN decomposition reaction.

The radical obtained in the first step of initiation (R*) reacts with a monomer, producing propagation radicals ($P_n\cdot$) (Scheme 1.3 – A). The particularity of RAFT polymerization is found in the propagation step, where chain activation/deactivation equilibrium takes place. In this case, the propagation radical ($P_n\cdot$) binds to RAFT agent by its addition into the thiocarbonyl group of the dithioester (Scheme 1.3 – B.1), generating intermediate radicals (Scheme 1.3 – B.2). The decomposition of the intermediate radicals yields a polymeric dithioester and the R group release (Scheme 1.3 – B.3). Then, the R group reinitiates the cycle by reacting with a monomer molecule, originating a new propagation radical ($P_m\cdot$) (Scheme 1.3 – C). At this point, an equilibrium between propagating radicals ($P_n\cdot$ and $P_m\cdot$) and the dormant forms (Scheme 1.3 – D.4) is established, allowing an excellent control over the polymeric chain growth, leading to a very narrow MW distribution. Finally, the termination occurs by the deactivation of the propagating chain without the formation of a new radical (Scheme 1.3 – E) (Favier *et al.*, 2006; Moad *et al.*, 2005; Odian, 2004; Vega-Rios *et al.*, 2011).

Some disadvantages can be identified in this procedure, since the polymers obtained by RAFT polymerization have the dithioester as end group which can be related with odors and colour. Several methods have been used in order to remove/transform the dithioester end group by hydrolysis, radical-induced reactions, thermal elimination or even UV radiation. Those transformations can be used in order to improve the obtained polymer properties according to its future application. Therefore, block copolymers and end functional polymers synthesis is possible by this method (Favier *et al.*, 2006; Moad *et al.*, 2005; Odian, 2004).

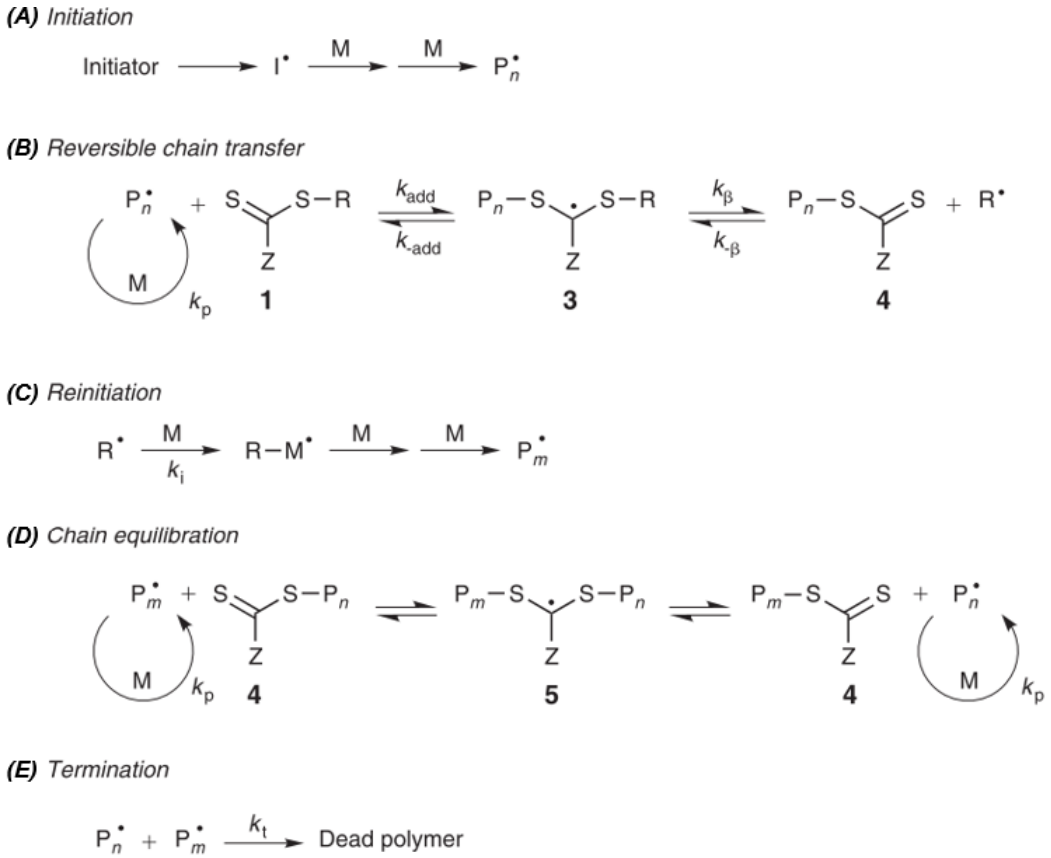

Scheme 1.2. RAFT polymerization mechanism (Moad *et al.*, 2005).

RAFT polymerization is of great interest due to the possibility of anchoring the CTA onto nanoparticle surface. This allows the polymers chains to grow from the core nanoparticles (*grafting from* method), obtaining polymer brushes grafted on the nanoparticle surface, with controlled thickness and high grafting polymeric density (Huang *et al.*, 2011; Santiago *et al.*, 2015).

1.6. Objective

The aim of this work was to develop and characterize hybrid mesoporous silica nanoparticles with silica nanostructured core and a shell of pH-responsive polymer. The biocompatible polymer used is based on a polybase tertiary amine methacrylate monomer known as 2-(diisopropylamino)ethyl methacrylate (DPAEM or DPA). A high quantum yield fluorescent perylenediimide (PDI) dye was incorporated into the MSN pore structure, for monitoring the MSNs, combining diagnostic and therapeutic properties on a single vector (Ribeiro *et al.*, 2013; Santiago *et al.*, 2015).

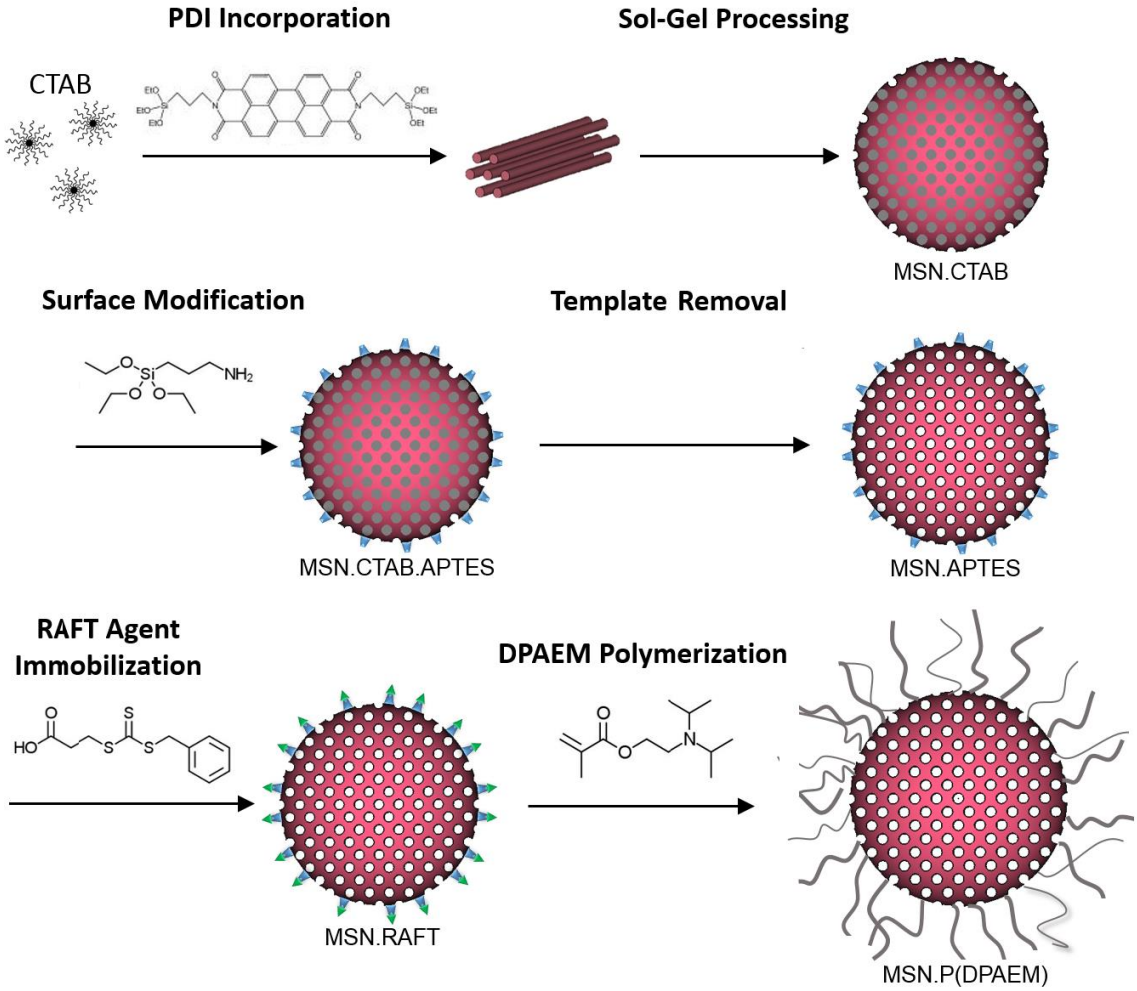

Figure 1.13. Schematic illustration for hybrid mesoporous silica nanoparticles prepared during this project.

The MSNs were synthesized, as described in figure 1.13, by the hydrolysis and condensation of tetraethoxysilane (TEOS) around hexadecyltrimethylammonium bromide (CTAB), used as surfactant, micelles with perylenediimide (PDI) adsorbed in its structure, obtaining fluorescent MSNs (Rodrigues *et al.*, 2013; Zhao *et al.*, 2009). Then, an amino surface modification was performed with (3-Aminopropyl) triethoxysilane (APTES) (Rodrigues *et al.*, 2013; Santiago *et al.*, 2015), followed by surfactant removal, ensuring the availability of the porous for later molecule incorporation (Ahmadi *et al.*, 2014; Rodrigues *et al.*, 2013; Vallet-Regí, 2012).

After that, CTA immobilization on MSNs surface was executed by attaching the carboxylic group of the CTA to the amine group located on MSN surface covalently, using a specific CTA (3- (benzylsulfanylthiocarbonylsulfanyl) propionic acid) in order to initiate a controlled 2-(diisopropylamino)ethyl methacrylate (DPAEM) monomer polymerization from the surface. This procedure is known as *grafting from*. This process allows hybrid MSNs synthesis with great polymeric density, distribution and controlled thickness, obtaining MSN.P(DPAEM) (Gao *et al.*, 2009; Ma *et al.*, 2014; Santiago *et al.*, 2015).

In order to characterize and verify the efficiency of *grafting from* procedure, some modifications of the procedure of polymer attachment to MSNs surface were performed. 2-(diisopropylamino)ethyl methacrylate RAFT polymerization was accomplished without nanoparticles on the same conditions and attached, posteriorly, to the MSNs surface. Such procedure is known as *grafting to* approach. The same CTA composed by a reactive group on its end chain that links covalently to the MSNs surface was also used. The polymer used for coating MSN, poly(2-(diisopropylamino)ethyl methacrylate) (PDPAEM), is highly biocompatible and pH sensitive, with pK_a around 6.5.

This hybrid system is a perfect candidate as drug delivery system with interesting applications on cancer treatment. It is known that tumor tissues present an acidic pH (around 6.5) contrasting to the normal tissues which pH is around 7.2. This type of systems are able to take advantage of the conformational transition of this polymer since its transition occurs in between these pH values. The mechanism expected for controlled drug release is illustrated in figure 1.14. In a basic/neutral medium (pH > 6.2), the polymeric shell exhibits hydrophobic behaviour due to its deionization, allowing a collapsed (unswollen) conformation that protects the drug loaded inside the MSN pores from diffusion. On the other hand, when the medium turns acidic (pH < 6.2), the polymer ionizes turning into a cationic soluble polyelectrolyte due to the protonation of its amine, showing an extended (swollen) conformation, that allows a gradual diffusion of the drug molecule into the medium.

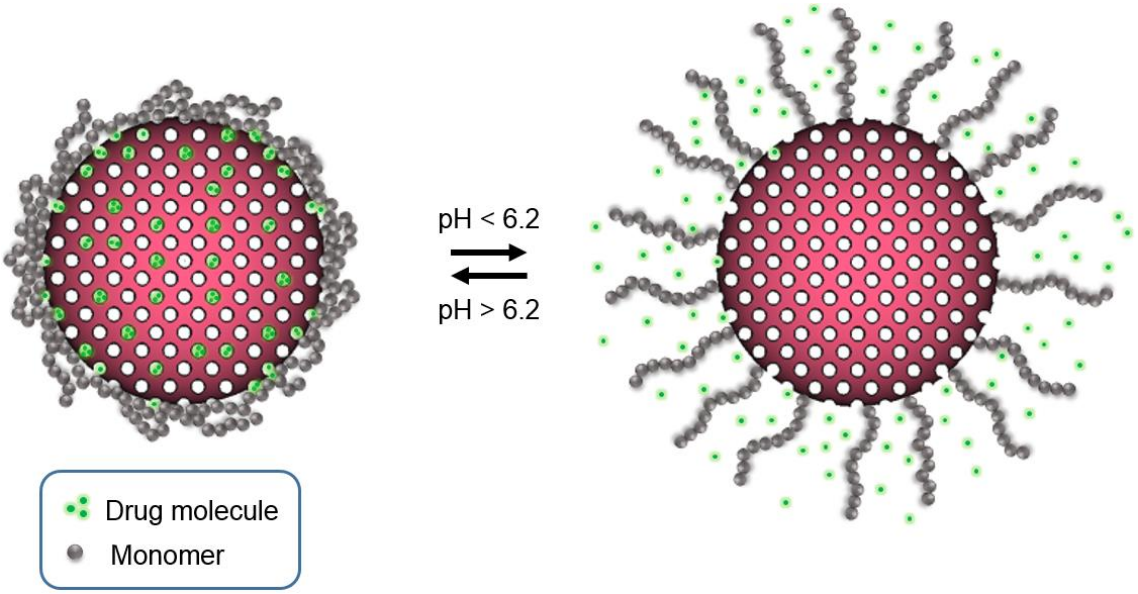

Figure 1.14. Schematic illustration of controlled drug release by MSN.P(DPAEM).

Transmission Electronic Microscopy (TEM) and Dynamic Light Scattering (DLS) techniques were used to characterize MSN and MSN.P(DPAEM) dimension and polydispersity. H^1 NMR was performed in order to verify and quantify APTES functionalization, to characterize the synthesized monomer and polymer as well as to verify its presence after being attached to the particles. UV-Visible Spectroscopy was necessary to quantify CTA as well as to determine P(DPAEM) pH response behaviour. FT-IR Spectroscopy was analyzed for qualitative characterization of the hybrid system. Lastly, ζ-Potential (ZP) technique was used, not only to determine surface charge changes along the surface modification process, but also to understand the charge transition with the pH.

2. Materials and Methods

2.1. Materials

Absolute Ethanol (99.9 % EtOH, Scharlau, Barcelona, Spain), hexadecyltrimethylammonium bromide (99 % CTAB, Sigma, St. Louis, MO, USA), sodium hydroxide (Pure NaOH, EKA Pellets, Bohus, Sweden) and tetraethoxysilane (99 % TEOS, Aldrich, St. Louis, MO, USA) were all used as received for synthesis of mesoporous silica nanoparticles (MSNs). The deionized (DI) water was generated using a Millipore Milli-Q system (≥18 MΩcm, Merck, NJ, USA). The dye incorporated into MSNs, PDI derivative, was synthesized according to the literature (Luo & Lin, 2006).

(3-Aminopropyl) triethoxysilane (98 % APTES, Sigma-Aldrich), without any treatment, was used for surface modification in dry toluene which was distilled over calcium hydride before use. The surfactant templates were removed using a 0.5 M hydrochloric acid solution (37 % HCl, AnalaR NORMAPUR - VWR, Radnor, Pennsylvania) in absolute EtOH.

For chain transfer agent (CTA) immobilization N-(3-dimethylaminopropyl) -N′-ethylcarbodiimide (98 % EDC, Sigma-Aldrich) in commercial distilled dichloromethane and 3-(benzylsulfanylthiocarbonylsulfanyl) propionic acid as CTA, synthesized according to the literature (Stenzel *et al.*, 2003), were used.

In order to synthesize the monomer 2–(diisopropylamino) ethyl methacrylate, hydroquinone (99 %, Aldrich Chemistry), methacryloyl chloride (97 %, Aldrich), and 2–(diisopropylamino) ethanol (98 %, Aldrich Chemistry) were all used as received. Also, tetrahydrofuran (99 % THF, Aldrich) distilled with sodium and dry triethylamine distilled over calcium hydride were used.

Lastly, for 2–(diisopropylamino) ethyl methacrylate (DPAEM) RAFT polymerization tetrahydrofuran (99.9 % TFA, Aldrich), azobisisobutyronitrile (AIBN pure) synthesized as described in the literature and 1,4 - Dioxane previously dried with sodium and distilled were used.

The samples preparation for DLS and ζ-Potential measurement required 3 mL plastic syringes (B-BRAUN, Germany), sodium dodecyl sulphate (98 % SDS, Aldrich) and cellulose 0.45 µm cellulose filters (VWR). Disposable capillary cells (DTS1070) (Malvern Instruments, Worcestershire, UK) were used for ζ-Potential measurements and disposable polystyrene cuvettes (Brand GMBH, Germany) for DLS measurement. TEM images were acquired by preparing well-dispersed MSNs and MSN.P(DPAEM) samples and placed in carbon grid (Ted Pella, USA) by using iTEM software.

For pH-response assays phosphate buffer solution (PBS) was prepared with sodium phosphate monobasic (98 % NaH_2PO_4, PanReac AppliChem, Barcelona, Spain) and sodium hydroxide (98 % NaOH, Sigma-Aldrich).

Chloroform-D (99.8 %, Cambridge Isotope Laboratories, MA, USA) and deuterium oxide (D_2O 99.9 %, Cambridge Isotope Laboratories), supplemented with NaOH and 1,3,5-trioxane (99.0 %, Fluka, Germany) or PBS, were used for quantitative and qualitative characterization by H^1 NMR. UV- Visible Spectroscopy was performed using MSN sample dispersion in quartz cuvettes (Hellma Analytics, Müllheim, Germany) with 1 cm x 1 cm dimension. Potassium bromide (KBr 99 %, Aldrich) was used to prepare pellet for FT-IR Spectroscopy.

For *in vitro* studies human mammary carcinoma cell line MCF-7 from European Collection of Authenticated Cell Cultures (ECACC), Dulbecco's Modified Eagle's medium (DMEM, Thermo Fisher Scientific, Massachusetts, USA), Fetal Bovine Serum (FBS, Thermo Fisher Scientific), Penicillin-Streptomycin (Thermo Fisher Scientific) and Thiazolyl Blue Tetrazolium Bromide (MTT, Sigma-Aldrich) were used. HCl (PanReac AppliChem), 2-propanol (PanReac AppliChem), Nonidet P-40 (NP40, Sigma) and Dulbecco's phosphate-buffered saline (DPBS, Thermo Fisher Scientific) were needed to prepare MTT solution and MTT solvent. For cell viability assay cells were seeded onto the 96 well plates (Corning, New York, USA).

2.2. Equipment

2.2.1. Centrifuge

Avanti J – 30I Centrifuge (Beckman Coulter, California, USA), rotor JA – 30.50 Ti, was used for washing MSNs. For the centrifugations, 50 mL centrifuge tubes from the same manufacturer were used. Centrifugal Refrigerator (3-16K) (Sigma Zentrifugen, Osterode am Harz Germany), rotor 12141, was used for washing MSN.PDPAEM. Disposable 10 mL polypropylene tubes were used for the centrifugations. At the end of the washing process of every MSNs modification procedure, a sample was taken into a 1.5 mL eppendorf for posterior.

2.2.2. Transmission Electronic Microscopy (TEM)

TEM images were obtained on a Hitachi transmission electron microscope (Hitachi High – technologies, Tokyo, Japan), model H-8100, with a LaB_6 filament (Hitachi) complemented with an accelerator voltage of 200 kV. A camera KeenView (Soft Imaging System, Münster, Germany) is incorporated in this equipment, which through iTEM software, allows acquiring TEM images. The size/dimension, polydispersity, and morphology of the particles were estimated by evaluating at least 100 nanoparticles by Image J software.

2.2.3. Dynamic Light Scattering (DLS) and ζ-potential

Zetasizer Nano ZS (Malvern Instruments, UK), model ZEN3600, with 173º and 90º detector was used in order to determine hydrodynamic particle radii in solution. The estimation of the nanoparticles size is based on the dynamic light scattering (DLS) assuming a Brownian movement of nanoparticles.

2.2.4. Rotary Evaporator

In order to evaporate the solvent on DPA synthesis a Heidolph – Laborota 4000 – Efficient (Sigma- Aldrich) was used at 313 K and 150 rpm.

2.2.5. UV-Vis Spectroscopy

UV-660 UV-VIS Spectrophotometer (JASCO International, Tokyo, Japan), supplied with a double monochromator and a photomultiplier detector for higher resolution, was employed for UV-Vis spectroscopy assays and cell viability assays.

2.2.6. ^{1}H NMR

Proton Nuclear Magnetic Resonance (^{1}H NMR) (δH) spectra were recorded on an AMX-400 instrument (Bruker, MA, USA).

2.2.7. FT-IR Spectroscopy

The Nicolet Impact 400D FT-IR Infrared Spectrophotometer (LabX, Midland, Canada) was used for FT-IR spectroscopy assays.

2.3. Methods

2.3.1. Mesoporous Silica Nanoparticles Synthesis

MSNs were synthesized by a sol–gel modified process. In a 500 mL polypropylene flask, 0.5 g of CTAB were dissolved in 240 mL of deionized water. Then, 1.75 mL NaOH with the desired concentration (1.40 M or 1.70 M) and 2.5 mL TEOS (0.88 M) were added dropwise under vigorous stirring at 353 K and left aged for 2 h. The MSNs were recovered by centrifugation at 30,000 x g for 10 min at 288 K, and washed three times with distilled water, discarding each time the supernatant. The solid product obtained by centrifugation was dried at 323 K overnight.

For perylenediimide (PDI) incorporated mesoporous silica nanoparticles (MSN.PDI), a solution of CTAB (0.5 g) and PDI (6 mg) in 2.5 mL THF was prepared in a 15 mL polypropylene flask and was left stirring at room temperature until THF be evaporated (approximately 24 h). The obtained solid was transferred to a 500 mL polypropylene flask and the same protocol described before was executed.

2.3.2. Mesoporous Silica Nanoparticles Surface Modification

Amino modification of the silica surface was performed by suspending the obtained nanoparticles in dry toluene (10 mL toluene per 200 mg of MSN) and sonicating it for 15 min. Afterwards, (3-aminopropyl) triethoxysilane (APTES) was added dropwise (0.468 mL per 200 mg of MSN). The resulting dispersion was heated at 398 K under reflux for 24 h in an argon atmosphere. Finally, the MSN.APTES were recovered by centrifugation at 30,000 x g for 10 min at 288 K, and washed one time with dichloromethane and three times with absolute ethanol, discarding each time the supernatant. The solid product obtained by centrifugation was dried at 323 K overnight.

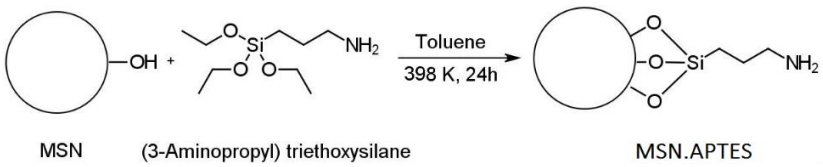

Figure 2.1. APTES surface modification scheme.

An acidic ethanol solution (0.5 M HCl, 20 mL of acidic solution for each 500 mg of MSN) was used to remove surfactant template, by re-suspending MSN.APTES on this solution and sonicating it. Subsequently, it was left under stirring at 313 K for 24 h. MSN were recovered by centrifugation at 30,000 x g for 10 min at 288 K, and washed four times with absolute ethanol, discarding each time the supernatant. The solid product obtained by centrifugation was dried at 323 K overnight.

In order to immobilize CTA on the nanoparticles' surface 10 mL of dry dichloromethane was added for each 500 mg of MSN into a 25 mL flask under the argon atmosphere and sonicated for 20 min. Then, 0.136 g of 3-(benzylsulfanylthiocarbonylsulfanyl) propionic acid (1 Eq APTES) and 0.106 mL of EDC (1.2 Eq APTES) were added to the mixture at 273 K, which was left under stirring with ice at room temperature for 24 h. MSN.RAFT were recovered by centrifugation at 30,000 x g for 10 min at 288 K, and washed three times with absolute ethanol, discarding each time the supernatant. The solid product obtained by centrifugation was dried at 323 K overnight.

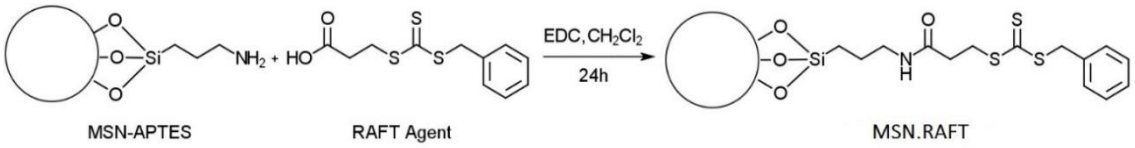

Figure 2.2. CTA Immobilization scheme on MSN surface.

2.3.3. 2 – (Diisopropylamino) ethyl methacrylate Monomer Synthesis

To a solution of hydroquinone (40 mg) in THF (40 mL) under argon atmosphere was added dry triethylamine (4 mL, 28 mmol, 1 Eq) and 2- (diisopropylamino) ethanol (4.8 mL, 28 mmol, 1 Eq) and stirred on ice. Afterwards, methacryloyl chloride (2.8 mL, 28 mmol, 1 Eq) was added dropwise and the mixture was left under stirring on ice at room temperature for 24 h. The product of the reaction was filtered on vacuum and the solvent was evaporated until an oil was obtained. Lastly, in order to separate the reaction intermediates from the monomer, the oil was distilled at 387 K on the vacuum.

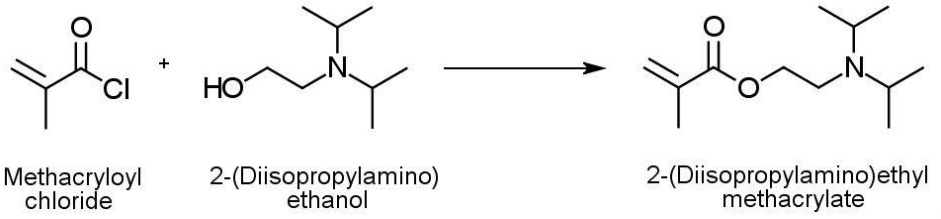

Figure 2.3. Condensation reaction.

2.3.4. *Grafting from*: RAFT Polymerization at the MSN Surface

In a schlenk tube A MSN.RAFT (50 mg), AIBN (1:10 AIBN/RAFT) and a magnet were added and placed in the vacuum. In a schlenk tube B 3 mL of 1, 4 – Dioxane, DPA, and TFA as described In table 2.1 was added. Atmosphere oxygen was removed from schlenk tube B through freeze-pump taw (4 to 5 cycles of freeze with vacuum and defreeze). The content of schlenk tube B was transferred to the schlenk tube A with the help of a cannula and argon. After that, the mixture was sonicated for 3 min and placed on a plate under stirring in the following conditions:

Table 2.1. Temperature, time and TFA equivalent used for the different polymerization reactions.

Polymerization Reaction		Temperature (K)	Time (h)	TFA (Eq)	DPA (Eq)
P(DPAEM) I		343	20		100
P(DPAEM) II		343	22	1.2	100
MSN.P(DPAEM) I		353	20		100
MSN.P(DPAEM) II	a	343	20		100
	b			1.2	
MSN.P(DPAEM) III	a	343	20		200
	b			1.2	

MSN were recovered by centrifugation at 30,000 x g for 10 min at 288 K, and washed three times with absolute ethanol, discarding each time the supernatant. The solid product obtained by centrifugation was dried at 323 K overnight.

2.3.5. *Grafting to*: Polymer immobilization at the MSN Surface

For polymer synthesis the same procedure as described for 2 – (Diisopropylamino) ethyl methacrylate RAFT Polymerization from Surface Nanoparticle (see 3.3.4) with the difference that in schlenk tube A instead of MSN, the same quantity of RAFT proportional to 50 mg of MSN was added. The polymer was suspended in dichloromethane and precipitated with diethyl ether for two days. The supernatant was discarded and the remaining diethyl ether was evaporated.

To immobilize P(DPAEM) on the MSN surface, the same procedure used for RAFT immobilization was used (see 3.3.2). In this case, instead of 1 Eq of CTA, 1:1 P(DPAEM) chain/APTES was added to the reaction.

3. Results and Discussion

3.1. MSN Size Distribution

MSN size distribution was analyzed at a controlled temperature on TEM and DLS (293 K) in order to estimate their diameter in the same conditions. The concentration of the sample was 0.3 mg/mL in ethanol and water, for TEM and DLS measurements, respectively. The samples prepared for TEM were well dried on a grid before its analysis.

For MSN synthesis, two different concentrations of NaOH were used (Table 3.1) in order to see the relation between diameter size and catalyst concentration, using the same conditions (temperature, stirring speed, surfactant, etc.) (Zhao *et al.*, 2009).

Table 3.1. Catalyst concentration (NaOH) used for the synthesis of each sample and its correspondent TEM image in figure 17.

SAMPLE	[NaOH] (M)	Figure 3.1
MSN A	1.7	A
MSN.PDI B	1.4	B
MSN C	1.4	C
MSN.PDI D	1.7	D
MSN E	1.4	E
MSN.PDI F	1.7	F

3.1.1. Transmission Electronic Microscopy (TEM)

For TEM size distribution analysis MSN dispersed in ethanol were prepared and dried on a carbon grid. Trough TEM image analyses it was possible to estimate the size distribution using Image J software by the measurement of a minimum MSN population of 100, excluding aggregates. In figure 3.1 we represent one TEM image of each sample, and the respective diameter distribution.

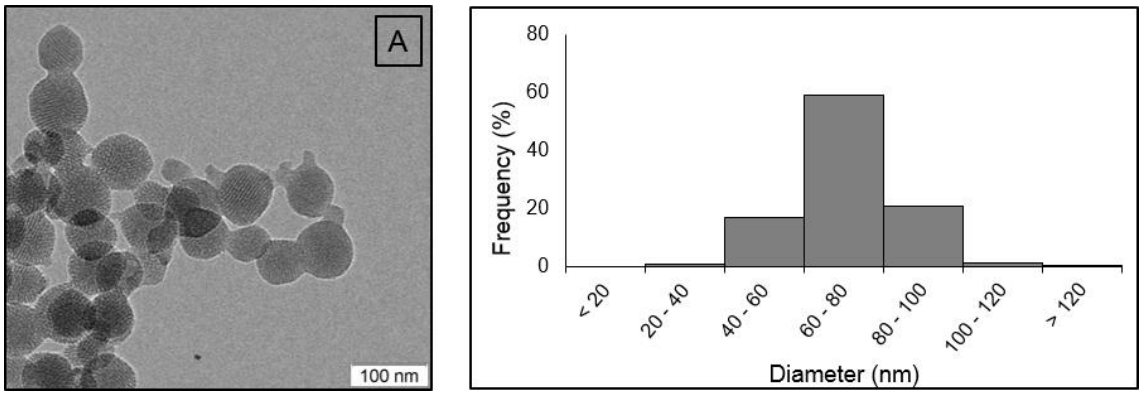

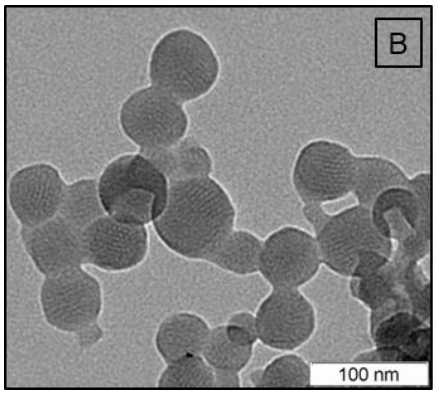
B
100 nm

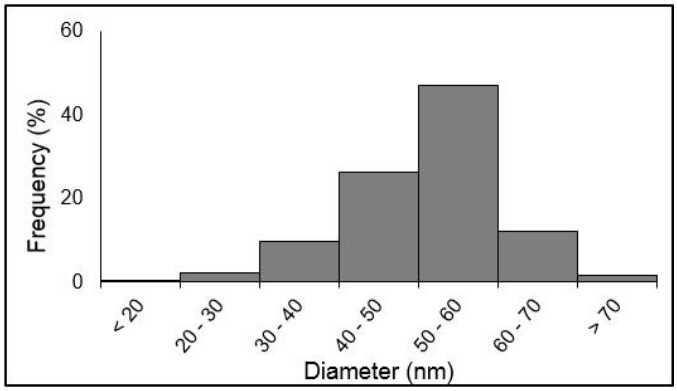
Frequency (%)
60
40
20
0
< 20
20 - 30
30 - 40
40 - 50
50 - 60
60 - 70
> 70
Diameter (nm)

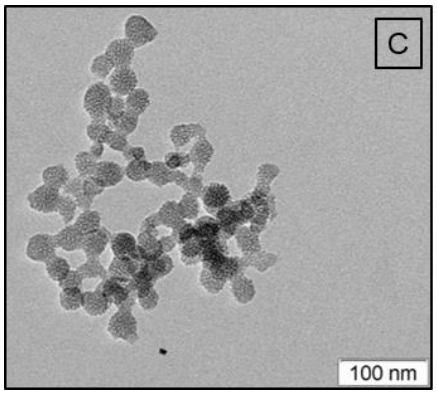
C
100 nm

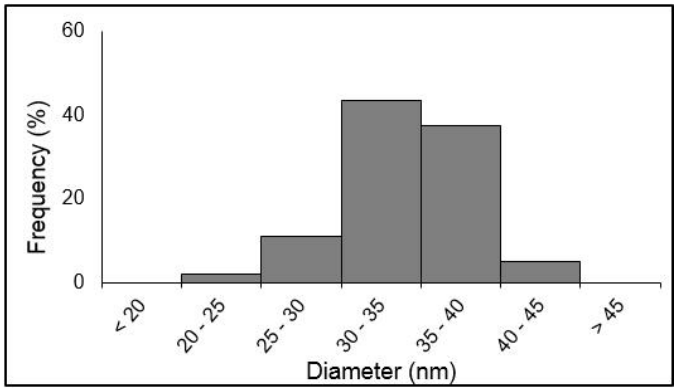
Frequency (%)
60
40
20
0
< 20
20 - 25
25 - 30
30 - 35
35 - 40
40 - 45
> 45
Diameter (nm)

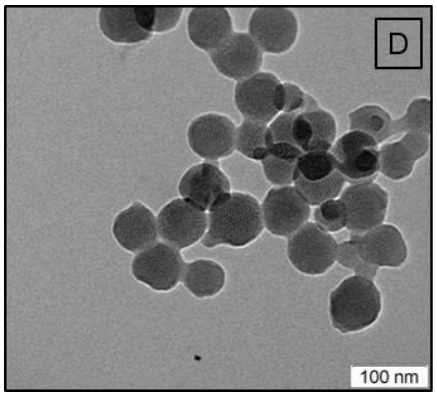
D
100 nm

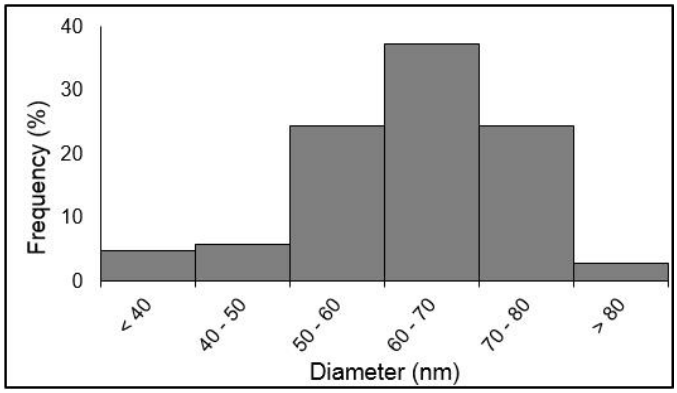
Frequency (%)
40
30
20
10
0
< 40
40 - 50
50 - 60
60 - 70
70 - 80
> 80
Diameter (nm)

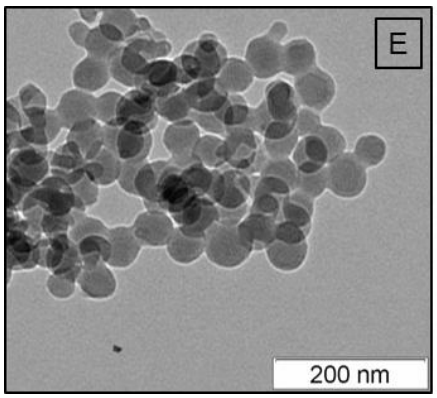
E
200 nm

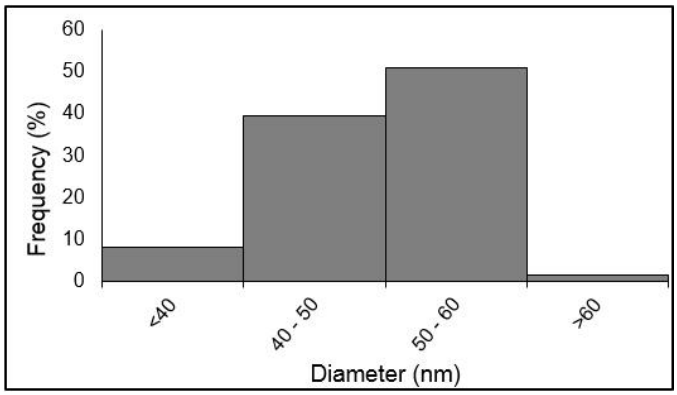
Frequency (%)
60
50
40
30
20
10
0
<40
40 - 50
50 - 60
>60
Diameter (nm)

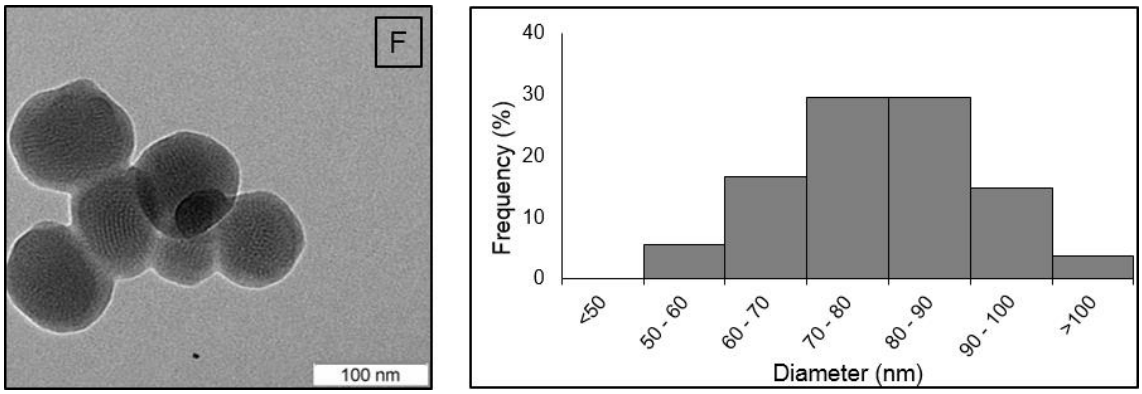

Figure 3.1. TEM images (100 nm scale) obtained for the nanoparticles synthesized (left) and its histogram size distribution (right). A: MSN A, B: MSN.PDI B, C: MSN C, D: MSN.PDI D, E: MSN E and F: MSN.PDI F.

This method allowed to obtain nanoparticles with a well-defined and organized mesostructure confirmed by TEM images obtained once the surfactant was removed (figure 3.2).

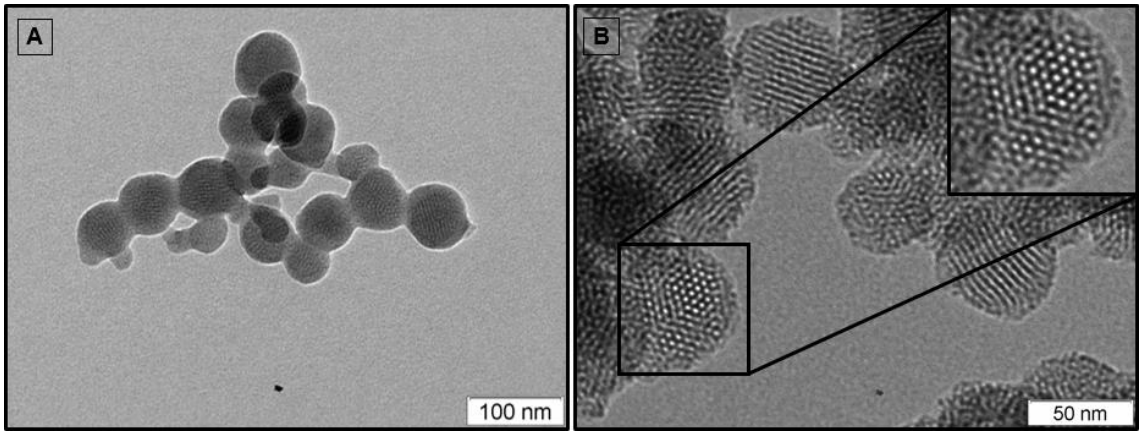

Figure 3.2. TEM images obtained for MSN.PDI D with surfactant (A) and for MSN.PDI D with surfactant removed (B) with a "zoom in" for better visualization of mesostructure.

3.1.2. Dynamic Light Scattering (DLS)

Dynamic Light Scattering (DLS) is a physical technique used to determine particles' size distribution profile in suspension or polymers in solution, assuming a Brownian motion. Brownian motion is the random motion of particles in a solvent. Using the Stokes-Einstein equation, it is possible to obtain the particle hydrodynamic diameter from the diffusion coefficient. Light scattering intensity fluctuations are analyzed an auto-correlation function. The results were analysed by the CONTIN method in order to determine nanoparticle hydrodynamic diameter (D_H). The hydrodynamic diameter was calculated from the average of three measurements. In table 3.2 the MSN diameter average and its standard deviation for DLS and TEM for every sample are described.

Table 3.2. MSN diameter average and its standard deviation obtained by DLS and TEM.

SAMPLE	[NaOH] (M)	D_H (nm)	D_{TEM} (nm)
MSN A	1.7	77 ± 30	71 ± 13
MSN B	1.4	63 ± 24	51 ± 10
MSN.PDI C	1.4	52 ± 20	35 ± 4
MSN.PDI D	1.7	87 ± 32	63 ± 11
MSN E	1.4	52 ± 27	50 ± 7
MSN.PDI F	1.7	153 ± 33	79 ± 12

It is possible to see that the diameter obtained by DLS is higher than the obtained by TEM analysis. This can be explained by the 1) hydrated layer around MSN when they are dispersed and 2) the tendency of the nanoparticles to form clusters.

The method used for MSN synthesis is promising since the nanoparticles obtained are on the ideal diameter range for targeting cancer cells (between 35 to 100 nm), with regular shape and narrow polydispersity in each synthesis. In addition, it was possible to obtain two ranges of diameter by using different NaOH concentration, one between 35 – 50 nm for 1.4 M NaOH and other between 60 – 80 nm for 1.7 M NaOH.

3.2. MSN Surface Modification Analysis

3.2.1. ^{1}H NMR

NMR spectroscopy is a fundamental tool that provides information about structure, composition, interactions and dynamic of organic molecules at atomic resolution. It can be used as a quantitative or qualitative method.

After MSN synthesis, an amino surface modification was performed by adding (3-aminopropyl) triethoxysilane (APTES) to the silanol group of the nanoparticle surface ^{1}H NMR was performed after this process in order to assess and quantify the immobilization of this compound (Slowing *et al.*, 2010). The samples were prepared in 500 µL of D_2O with a high concentration of NaOH, 0.5 mg of the sample and 0.5 mg of 1,3,5-trioxane and sonicated until obtain a transparent solution. This method is used to perform a better quantification of the molecules linked to the surface by destroying the MSNs. The molecules in solution have better mobility, obtaining a more defined ^{1}H NMR spectra (Crucho, *et al.*, 2016). In table 4.3 we show the estimated concentrations of APTES per gram of MSN.

Table 3.3. APTES concentration on the MSN surface, calculated by ^{1}H NMR.

SAMPLE	[APTES] (mmol/g MSN)
MSN A	1.78
MSN B	1.58
MSN.PDI C	1.64
MSN.PDI D	2.90
MSN E	2.45
MSN.PDI F	3.09

This amino modification allows the attachment of other functional groups or biomolecules. The MSN with surface APTES concentration lower than 1.60 mmol/g ensures less than 3 molecules per nm^2, creating an amine monolayer around the MSN. The nanoparticles with that concentration were preferentially used for further proceedings due to their homogeneity.

3.2.2. UV-Vis Spectroscopy

The immobilization of CTA on the MSNs surface is achieved by attaching the carboxylic group of the CTA to the amine group located on MSN surface covalently. In order to calculate the CTA concentration on the MSN surface, UV-Visible Spectroscopy was used. The RAFT agent, 3-(benzylsulfanylthiocarbonylsulfanyl) propionic acid, show a maximum absorbance near 310 nm wavelength (Santiago *et al.*, 2015). UV- Visible spectra of MSN with NH_2 group (previous step) and MSN with RAFT immobilized in the surface were measured. The samples were prepared with an initial concentration of 0.2 mg/mL in dioxane. In figure 3.3 it is shown the absorbance spectrum obtained for MSN A as an example, since the same procedure was applied to the other samples.

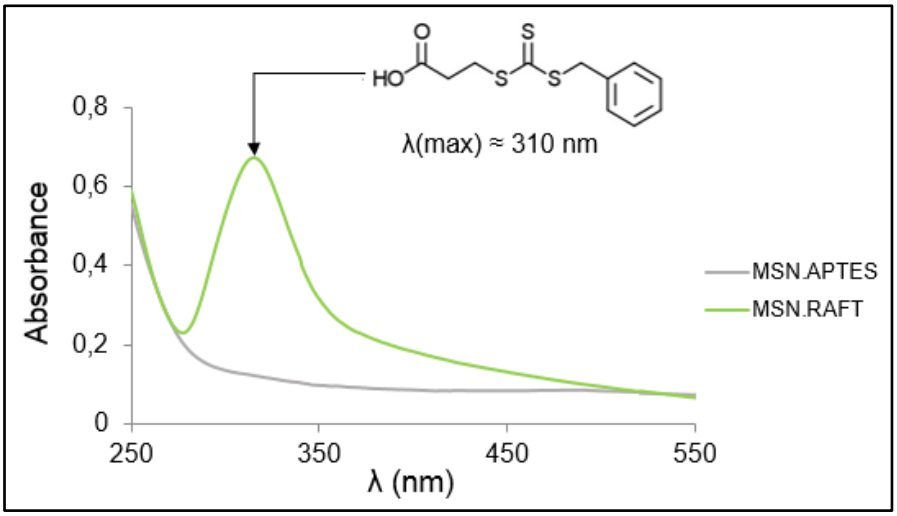

Figure 3.3. UV-Vis Spectrum for MSN.NH2 adjusted (grey) and for MSN.RAFT (on green).

The concentration was calculated through the Lambert-Beer law (Equation 4.1).

$$\mathrm{Abs} = \varepsilon \mathrm{cl} \qquad (3.1)$$

Where *A* is the absorbance, *ε* is the molar absorptivity ($mol^{-1}cm^{-1}$), *c* is the concentration and *l* the cell length (optical path). The absorbance used was the one obtained at λ = 310 nm from the correction of MSN.RAFT spectra from the silica nanoparticles scattering (MSN.NH_2 spectra).

The molar absorptivity used was the one obtained for the free RAFT agent in dioxane (ε = 13.976 $mmol^{-1}cm^{-1}$) (Santiago *et al.*, 2015) and the cell length (*l* = 1 cm). The RAFT concentrations obtained (table 3.4) correspond to a CTA surface density of approximately 1 CTA per nm^2 of the surface for MSN A and MSN B, and of 0.3 CTA per nm^2 for MSN E. The different results are explained by the excess of CTA agent used during the reaction to ensure its immobilization, over the development of this work some optimizations were performed.

Table 3.4. RAFT concentration calculated through the Lambert-Beer equation.

SAMPLE	[RAFT] (mmol/g MSN)
MSN A	5.45×10^{-1}
MSN D	5.73×10^{-1}
MSN E	2.04×10^{-1}

The determination of CTA concentration needs to be accurately calculated for the polymerization step, since the initiator quantity is defined by the ratio [AIBN]/[CTA], and this need to be precisely controlled due to its influence on the polymer chain size. An excess of initiator concentration would result in a lower polymer MW.

3.2.3. ζ-potential Determination

ζ-potential is related to the electric potential in the interfacial double layer (DL), i.e. the potential difference between the dispersion medium and the stationary layer “attached” to the dispersed particles. The absolute magnitude of the ζ-potential measures the degree of electrostatic repulsion between adjacent similar charged-carrying particles. Commonly, it is used to evaluate the stability of the colloidal dispersion. The higher the absolute ζ-potential value the higher the dispersion stability, since the repulsion force between similar particles is larger. It is a qualitative method that allows the evaluation of the surface charge modification at each stage (Bhattacharjee, 2016; Xu, 2008). The ζ-potential was measured (see Table 3.5) in every modification step of MSN, the surfactant being previously removed, in order to assess modifications on surface charge along the process, by dispersing 0.5 mg of the sample in 2 mL of milli-Q water (pH=5).

Table 3.5. ζ-potential of MSN samples on every step of its surface modification measure at pH=5.

SAMPLE	ZP (mV)		
	MSN	$MSN.NH_2$	MSN.RAFT
MSN A	-23.8	34.5	-15.3
MSN B	-22.7	28.3	
MSN.PDI C	-23.0	28.8	
MSN.PDI D	-25.5	30.0	8.73
MSN E	-20.8	30.8	-17.5
MSN.PDI F	-24.9	29.9	

It is possible to observe a ζ-Potential change trend in every surface modification step. MSN show negative potential since the silanol groups have an isoelectric point (IEP) of 1.5, having a negative charge on its surface at pH superior to 1.5 (Rosenholm *et al.*, 2008; Ross *et al.*, 2005; Santiago *et al.*, 2015). The amine-functionalized MSNs show positive potentials due to the aminopropyl groups, which have pk_a equal to 9.8, being protonated at pH under 9.8 (DeMuth *et al.*, 2011; Rosenholm *et al.*, 2008; Santiago *et al.*, 2015). The immobilization of CTA in the MSN surface resulted in a decrease into negative charges of ζ-Potential, which indicates a successful surface modification (Santiago *et al.*, 2015). The result obtained for MSN.PDI B the suggest remain surfactant that contribute to a positive value.

3.3. Monomer and Polymer Characterization

3.3.1. ^{1}H NMR

The synthesis of 2 – (Diisopropylamino) ethyl methacrylate (DPAEM) was confirmed by ^{1}H NMR. In figure 3.4 it is shown the ^{1}H NMR spectra of the synthesized DPAEM. The DPAEM structure can be attributed to the peaks observed at 1.00 ppm (**a**, -(CH(C**H$_3$**)$_2$), 1.92 ppm (**e**, "methacrylic" C**H$_3$**), 2.66 ppm (**c**, -CH$_2$C**H$_2$**N-), 2.99 ppm (**b**, -(C**H**-N)$_2$-), 4.04 ppm (**d**, - OC**H$_2$**CH$_2$-), 5.52 ppm (**f**, -C**H** affected by the O electron cloud from the ester group) and 6.08 ppm (**g**, -C**H**). In addition, it is possible to detect the presence of the initial reagent 2- (diisopropylamino), as expected from the yellowish oil obtained, proven by the low intensity peaks with small deviation from the DPAEM peaks (a, b, c and d). The monomer was purified by distillation until a colorless oil was obtained. The relative yield of this synthesis procedure is about 65 – 70 %.

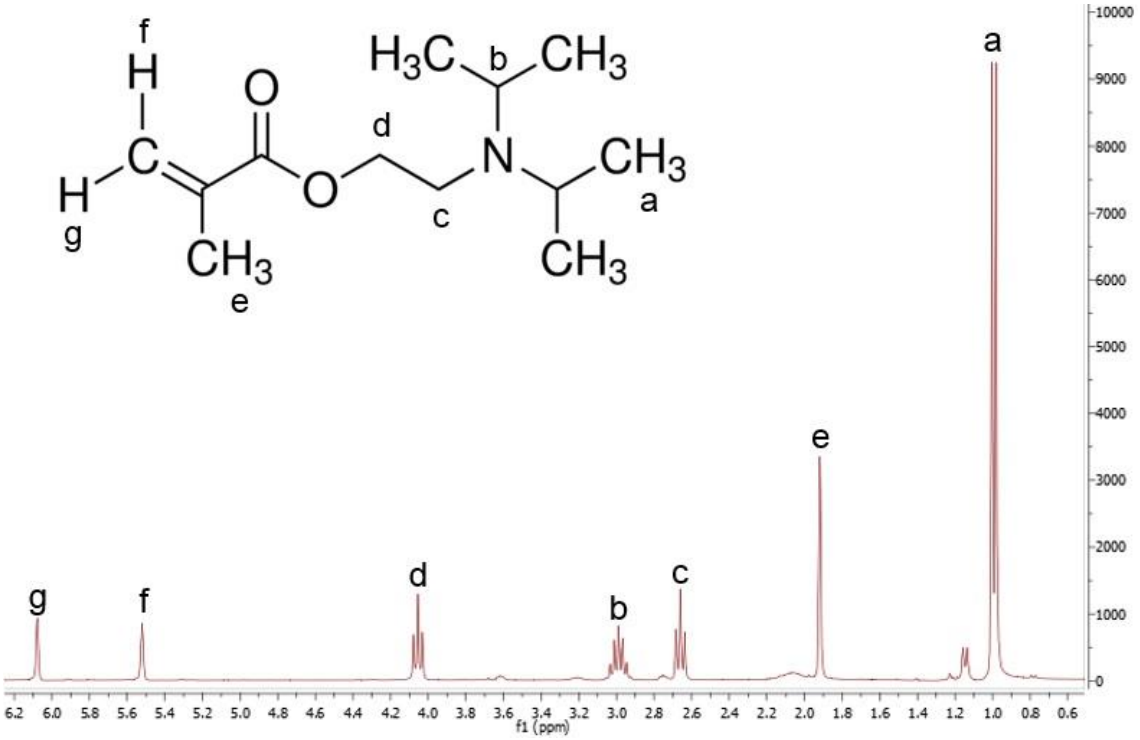

Figure 3.4. ^{1}H NMR spectra recorded at 400 MHz of DPAEM in chloroform.

^{1}H NMR spectroscopy also allowed to evaluate 2 – (Diisopropylamino) ethyl methacrylate RAFT polymerization assisted by 3-(benzylsulfanylthiocarbonylsulfanyl) propionic acid as CTA and determine the resultant chemistry structure. A ^{1}H NMR spectra of P(DPAEM) II sample dissolved in deuterated chloroform is shown in figure 3.5. The peaks observed at 1.00 ppm (**a**, -(CH(C**H$_3$**)$_2$; **e**, "methacrylic" C**H$_3$**; **f**, -C**H$_2$-** of the polymer backbone), 2.90 ppm (**c**, -CH$_2$C**H$_2$**N-), 3.28 ppm (**b**, -(C**H**-N)$_2$-) and 3.97 ppm (**d**, -OC**H$_2$**CH$_2$-) are in agreement with the P(DPAEM) structure (Góis *et al.*, 2014; Hu *et al.*, 2007). The enlargement of the signals when compared with the ^{1}H NMR spectra of DPAEM (figure 3.4) is an evidence of its polymerization, aside from the deviation from 1.92 to 1.00 ppm of the methacrylic CH$_3$ (**e**). The peak at 2,68 ppm (**h**, -SC**H$_2$**CH$_2$-; **i**, -C**H$_2$**COOH) belongs to the Z group of the RAFT agent. However, the total conversion of monomer to polymer was not achieved as shown by the presence of the signals at 1.54 ppm (**e***, "methacrylic" C**H$_3$**), 5.22 ppm (**f***, -C**H** affected by the O electrons from the ester group) and 5.74 ppm (**g***, -C**H**) associated with the monomer structure. The overlapping of polymer signals and the low intensity of the CTA resonances hindered the calculation of $M_{n,NMR}$. Nevertheless, the degree of polymerization was estimated through the correlation between the integral of **h** and **i** methylene protons at 3.09 ppm and **b** at 3.68 ppm (Góis *et al.*, 2014). From the ratio $4n/(n(2n)=I_i/I_f$, n=30.56 was obtained and so the estimation of the polymer molecular weight: $M_{n,NMR} = nM_{mon} + M_{CTA} \approx$ 7,064 Da. The theoretical M_n for this polymerization was nearly 21,600 Da per chain. The estimated yield for this reaction is 32.70 %.

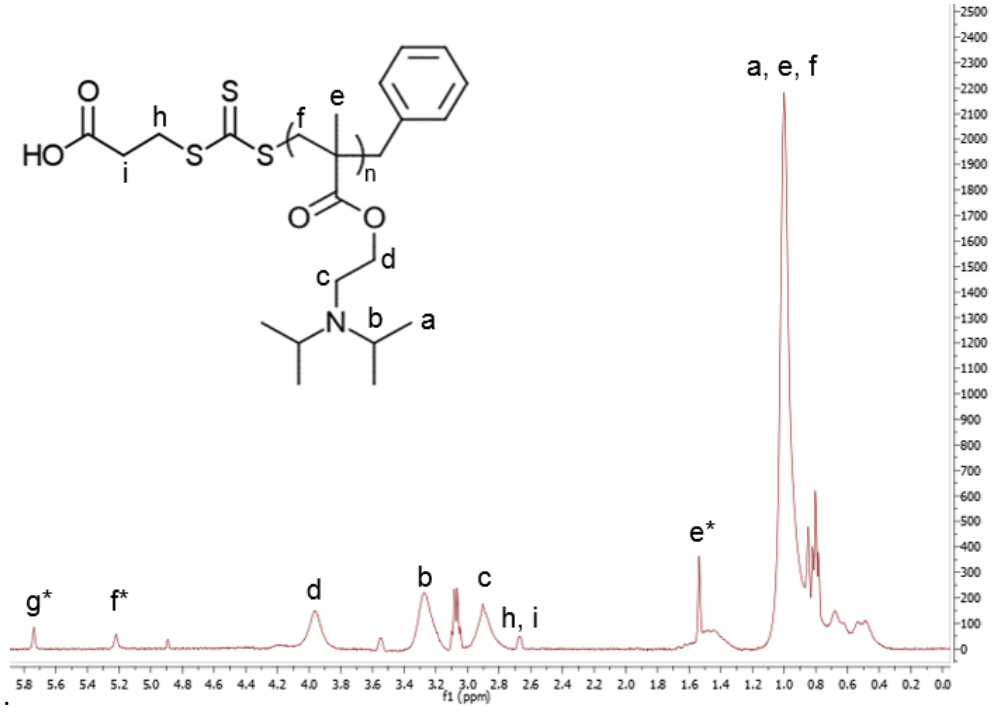

Figure 3.5. The ^{1}H NMR spectra recorded at 400 MHz of P(DPAEM) II prepared in chloroform.

Table 3.6. Monomer and CTA molecular weight used for calculate Mn,NMR

Compound	Symbol	MW (Da)
2 – (Diisopropylamino) ethyl methacrylate	M_{mon}	213.32
3-(benzylsulfanylthiocarbonylsulfanyl) propionic acid	M_{CTA}	272.41

3.3.2. UV-Vis Spectroscopy

The polymer pH response was characterized by the evaluation of the pH effects on optical transmittance. In figure 3.6 it is shown the spectrum obtained for the same sample prepared in phosphate-buffered saline (PBS) at different pH. It is possible to observe the optical transmittance difference between the extended conformation (pH lower than 6.5) and the collapsed conformation (pH higher than 6.3). The extreme decrease in optical transmittance at pH higher than 6.3 is caused by the deprotonation of the DPAEM units, becoming hydrophobic, and consequently precipitating (Peng *et al.*, 2010).

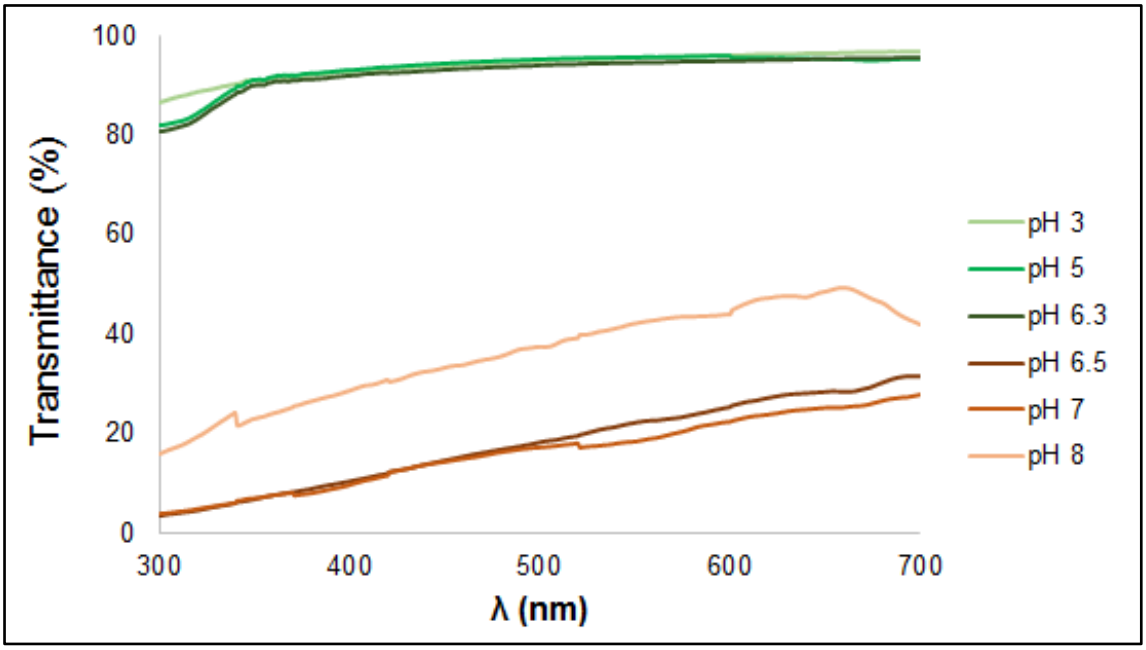

Figure 3.6. Transmittance spectrum for P(DPAEM) I sample at different pH.

In figure 3.7 we represent the transmittance variations at this wavelength as a function of pH. It was possible to see the decrease on transmittance values as the solution becomes more basic (Peng *et al.*, 2010). The reversibility of the transition phenomenon from hydrophobic state (collapsed conformation) to hydrophilic state (extended conformation) was evaluated by increasing the pH of an acidic solution of the sample, by adding dropwise 1 M NaOH, and decreasing the pH again, by adding 0.10 M HCl, measuring the transmittance for each pH. It was also possible to observe that the highest transmittance was reached once the pH of the sample decreased below the pK_a. These assays confirmed the reversibility of this transition.

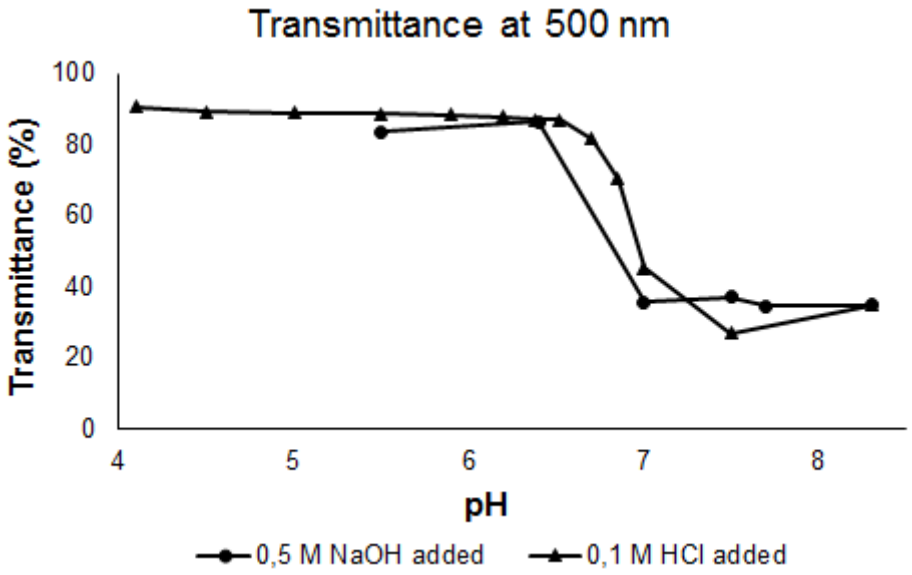

Figure 3.7. Transmittance at 500 nm of P(DPAEM) as a function of pH. The pH was increased by adding 1 M NaOH (●) and decreased by adding 0.1 M HCl (▲).

3.4. Hybrid Nanoparticles

3.4.1. Size Distribution

The hydrodynamic diameters for MSN.P(DPAEM) were determined by DLS in ethanol, milli-Q water and phosphate-buffered solution with different pH. We had some problems to obtain the size distribution of the samples due to the formation of aggregates in the used solvents. The samples were prepared with 1mg/mL and different dissolutions were tested. In order to compare with the results obtained for free MSN, the measurements were performed at 298 K.

The hydrodynamic diameters for MSN.P(DPAEM) determined by DLS are shown in table 3.7. It was not possible to reproduce the conditions of measurement for all the samples, due to aggregation of the particles. Nevertheless, the best results were obtained in milli-Q water at pH 5 with dissolution 1:3, confirming a size increase when compared with free MSN, which suggests the presence of a polymeric shell. These results are shown in Appendix A. The interactions between the polymeric chain could be the cause of the system instability, which could explain the results obtained for size distribution by intensity and number, as well as for their correlogram and cumulant fit, shown in Appendix B.

The diameters predicted by TEM analysis were calculated by the measurement of a population of 25 nanoparticles. The analysis of such low population emerges as a consequence of the samples preparation requirements due to the presence of polymer (such as short sonication time) not being possible to obtain a well dispersed sample. The results obtained are shown in table 3.7. By comparing these results with the ones obtained for free MSN samples it was possible to see a decrease on size diameter, which can be explained by low population analysis and the sedimentation of MSN.P(DPAEM) during the experiment.

Table 3.7. Average hydrodynamic diameter (D_H) obtained by DLS and the diameters obtained by TEM (D_{TEM}).

SAMPLE	D_H (nm)	D_{TEM} (nm)
MSN D.P(DPAEM) I	127 ± 49	59 ± 7
MSN E.P(DPAEM) II a	150 ± 51	
MSN E.P(DPAEM) II b	178 ± 48	43 ± 6
MSN E.P(DPAEM) III a		47 ± 5
MSN E.P(DPAEM) III b		46 ± 5
MSN C.G P(DPAEM) I		36 ± 6
MSN F.G P(DPAEM) I		67 ± 11

TEM images obtained are shown in figure 3.8. In images B, C and E a shadow can be noticed around the MSN core, which suggests the presence of the polymeric shell. Images A and D do not show polymeric shell probably as a consequence of the degradation of the polymer under the electron beam of TEM.

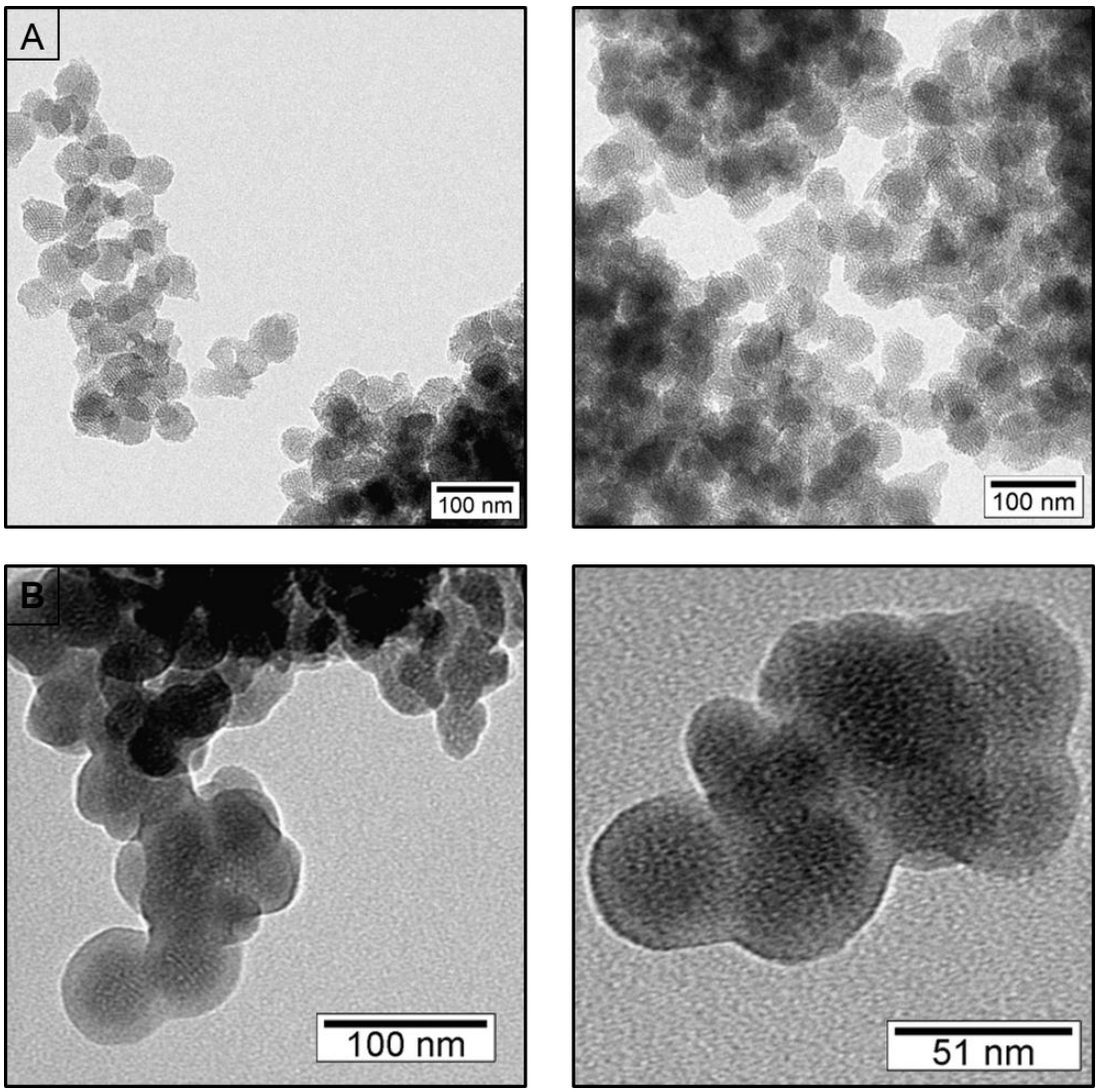

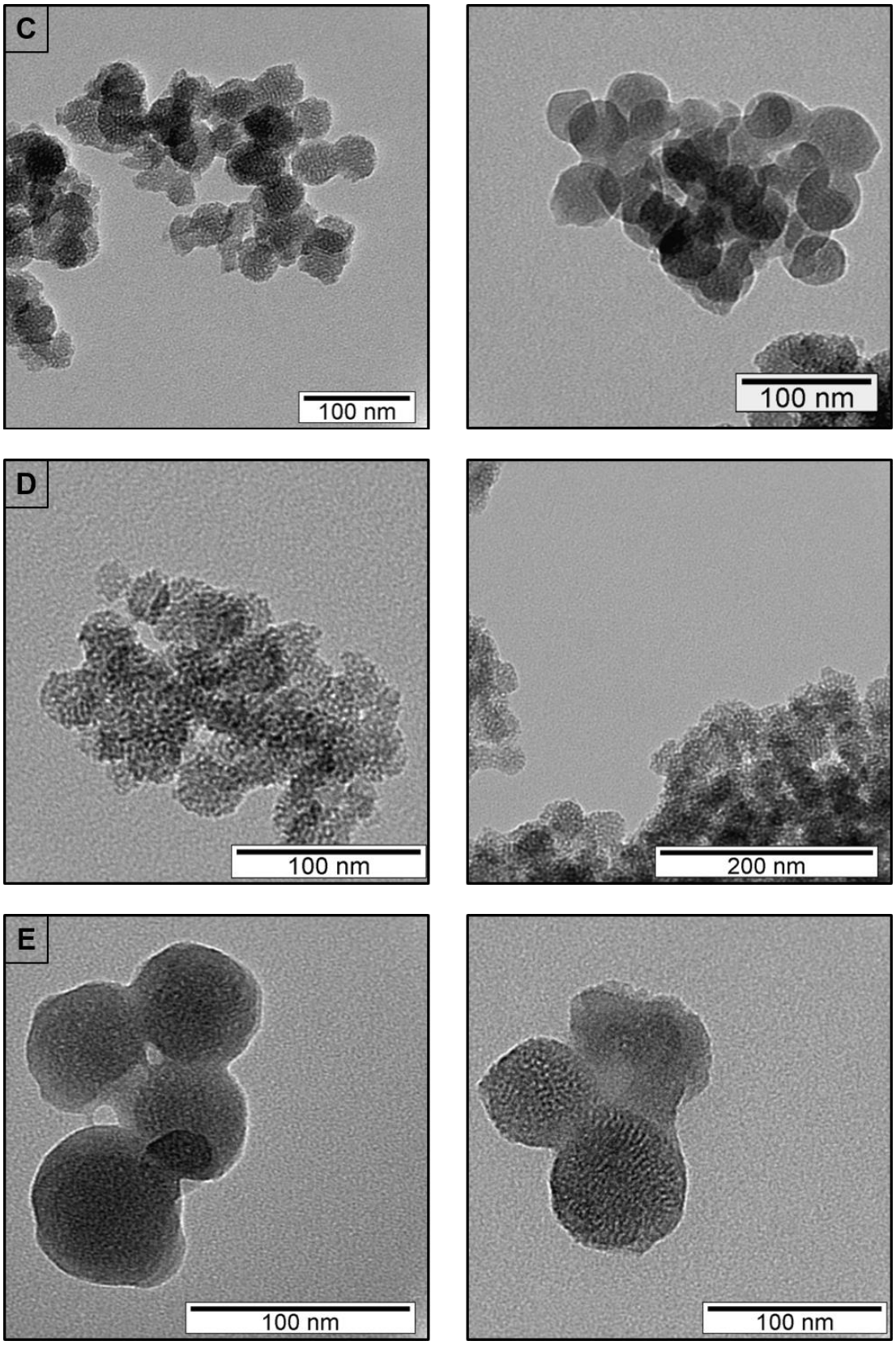

Figure 3.8. TEM images obtained for MSN D.P(DPAEM) I (A), MSN E.P(DPAEM) II b (B), MSN E.P(DPAEM) III a (C), MSN C.G P(DPAEM) I (D) and MSN F.G P(DPAEM) I (E).

The pH effect on the diameter size of the hybrid nanoparticle was studied by DLS, but it was not successfully concluded, due to the presence of agreggates (Appendix B).

3.4.2. ^{1}H NMR

^{1}H NMR was used to confirm the presence of P(DPAEM) presence at MSN surface, both for the hybrid nanoparticles obtained by *grafting from* (figure 3.9) or *grafting to* (figure 3.10) techniques. The samples were dispersed in D_2O supplemented with PBS to improve polymer solubility.

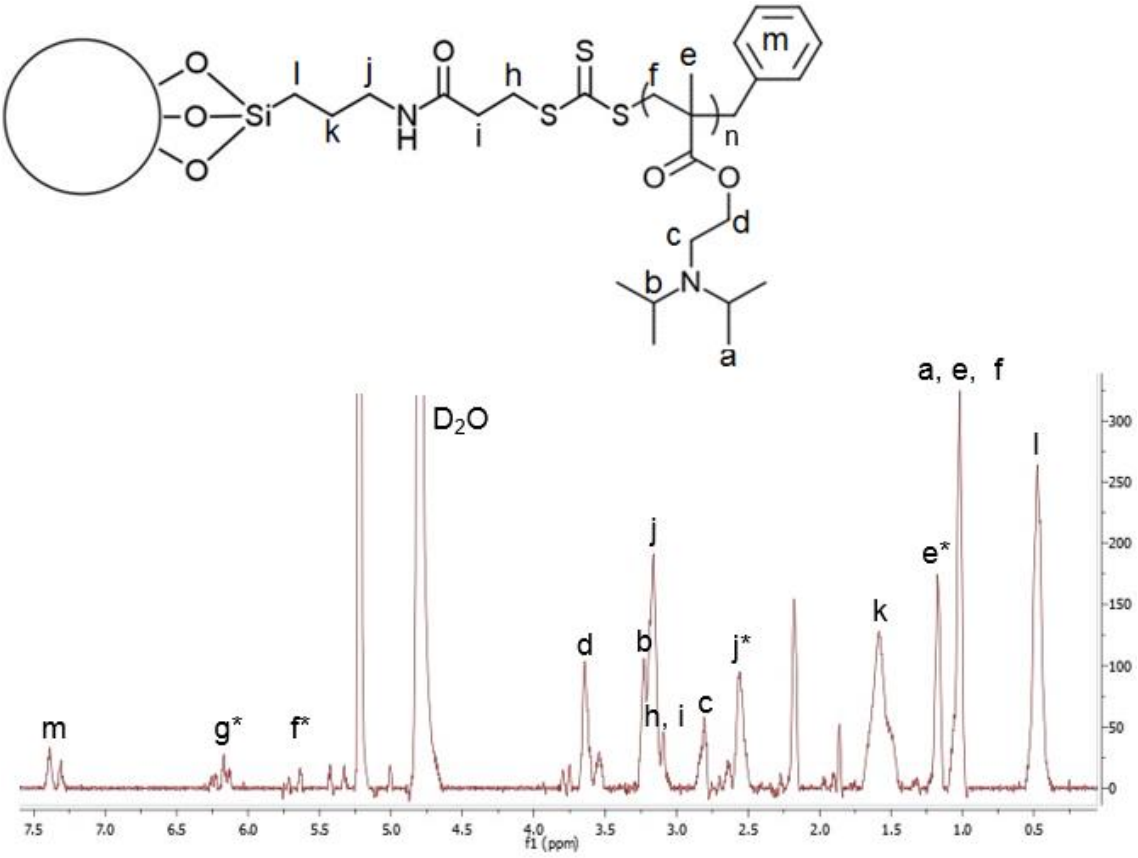

Figure 3.9. ^{1}H NMR spectrum for P(DPAEM) I *grafting from* polymerization on MSN B (MSN D.P(DPAEM) I).

In figure 3.9 the spectrum for MSN.P(DPAEM) I is shown as a representative ^{1}H NMR from all the polymerization performed by *grafting from* approach since there is such slight differences between them, mostly on the intensity of the peaks. Besides the peaks already attributed to the P(DPAEM) and free DPAEM (see 3.3.1), it was possible to confirm the presence of APTES covalently attached to CTA by the peaks approximately located at 0.46 ppm (**l**, -$O_3SiC\mathbf{H_2}CH_2$-), 1.57 ppm (**k**, -$C\mathbf{H_2}CH_2NH$-) and 3.15 ppm (**j**, -$CH_2C\mathbf{H_2}NH$-). This molecule was also present without any CTA attached, confirmed by the peak at 2.54 ppm (**j***, -$CH_2C\mathbf{H_2}NH_2$).

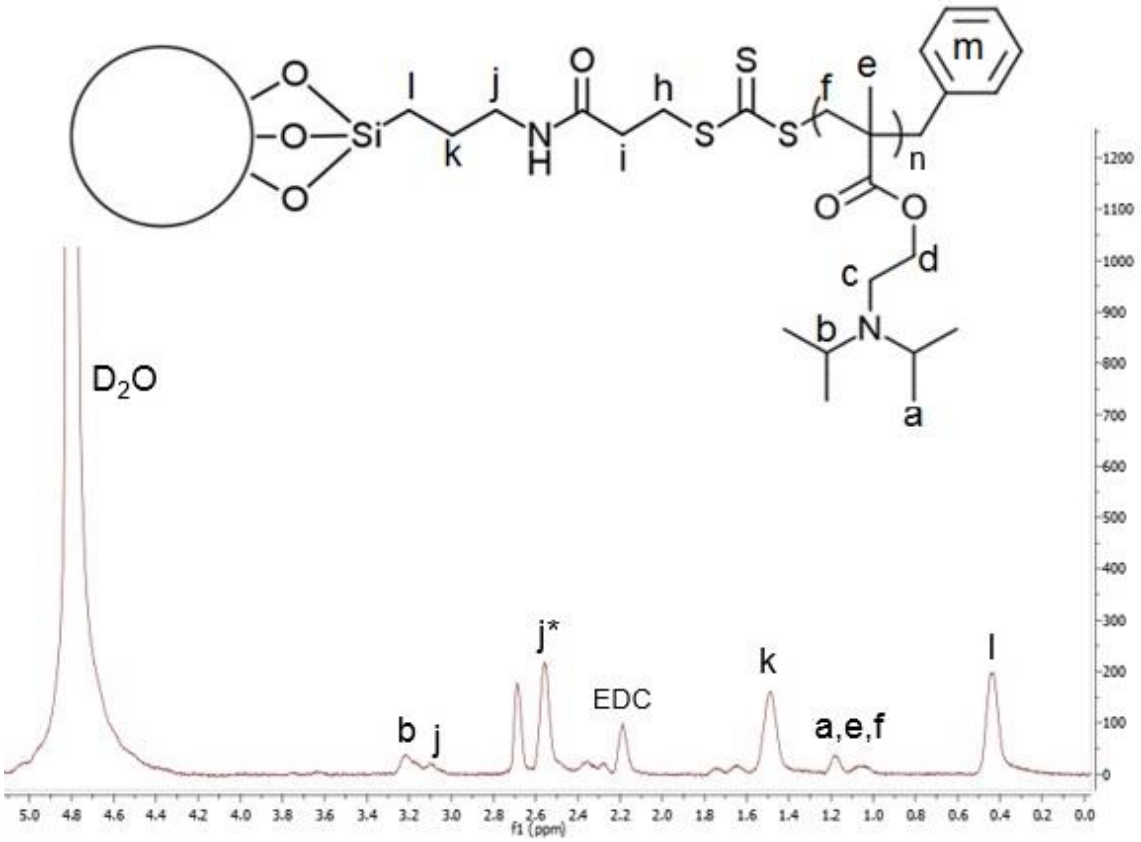

Figure 3.10. ^{1}H NMR spectra of P(DPAEM) I *grafting to* on MSN F surface (MSN F.G P(DPAEM) I).

In figure 3.10 the spectra recorded for MSN.G P(DPAEM) I, obtained by *grafting to* approach, is represented. It was not possible to identify the peaks attributed to the monomer, which is consistent with the method used, since the polymer was produced separately and then attached to the MSN surface. On the other hand, the small peaks present on the spectra could be attributed to CTA and polymer structure. In addition, most of the APTES molecule is in the free form, confirmed by the intensity of the peak at 2.58 ppm (j*). These two facts suggest an inefficient polymer attachment to the MSN surface. The signal at 2.21 ppm belongs to remaining EDC chemical, used to crosslink the carboxylic acid from the CTA to the primary amine from the APTES molecule.

3.4.3. FT-IR Spectroscopy

FT-IR Spectroscopy was used as a qualitative tool to assess MSN surface modification after RAFT polymerization. With this purpose, FT-IR spectra were recorded for the MSN samples before and after polymerization as well as for free polymer synthesized under the same conditions.

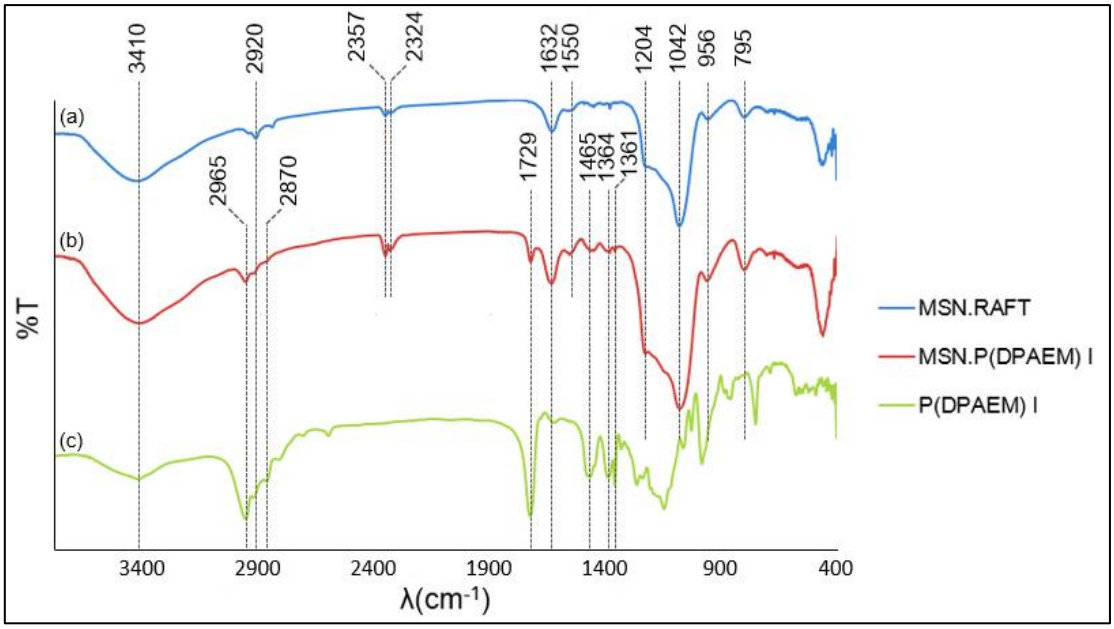

Figure 3.11. FT-IR spectra of MSN.RAFT (a), MSN.P(DPAEM) I (b) and free P(DPAEM) I (c) samples.

In figure 3.11 it is shown the FT-IR spectra for MSN.RAFT, MSN.P(DPAEM) I and P(DPAEM) I. The evaluation of surface modification was made through the comparison between the spectra obtained for MSN after RAFT polymerization with the polymer and the MSN before polymerization. The three spectra showed bands at 1632 cm^{-1} and at 3410 cm^{-1} which belong to the adsorbed water. Specifically, the one at 3410 cm^{-1} is characteristic of *v*(−OH) vibrations from the molecular water interacting by H-bonding with the carboxylic acid from RAFT agent present on the polymer and with the silanol groups located on the MSN surface. In both MSN's infrared spectra, the typical silica spectra was observed. The bands at 1204–1042 cm^{-1} and 795 cm^{-1} belong to the symmetrical and anti-symmetric vibrations of *v*(Si–O–Si) and the vibrational band at 956 cm^{-1} is characteristic of silanol groups *v*(Si–OH). In addition, the APTES surface modification can be proved by the presence of the band at 1550 cm^{-1} which is attributed to *v*(N–H) vibrations, while the bands at 2357 – 2324 cm^{-1} belong to the vibrations of *v*(–NCO) from the covalent bond between APTES and CTA, indicating a successful CTA surface immobilization. The bands at 2965 – 2870 cm^{-1} and 1465 cm^{-1} – 1361 cm^{-1} are assigned to the *v*(C–H) and *δ*(C–H) vibration from the alkyl chains of the polymer as well as of the functional groups present on MSN surface. Finally, the peak at 1729 cm^{-1} is attributed to the *v*(C=O) vibrations of the ester group from the monomer's methacrylate side (De Barros *et al.*, 2015; Faccia *et al.*, 2013; Zhang *et al.*, 2014). This result confirm a successful MSNs surface modification, as well as its coating with the polymeric shell.

3.4.4. ζ-Potential

ζ-potential measurements of the nanoparticles were also performed in PBS as a function of pH, in order to determine the electrokinetic charge of the hybrid system, as well as to compare with the previous surfaces modified. The expected electrokinetic charge for this system is described on figure 3.12. The IEP should be similar to the pK_a of the polymer alone, at which the conformational transition occurs.

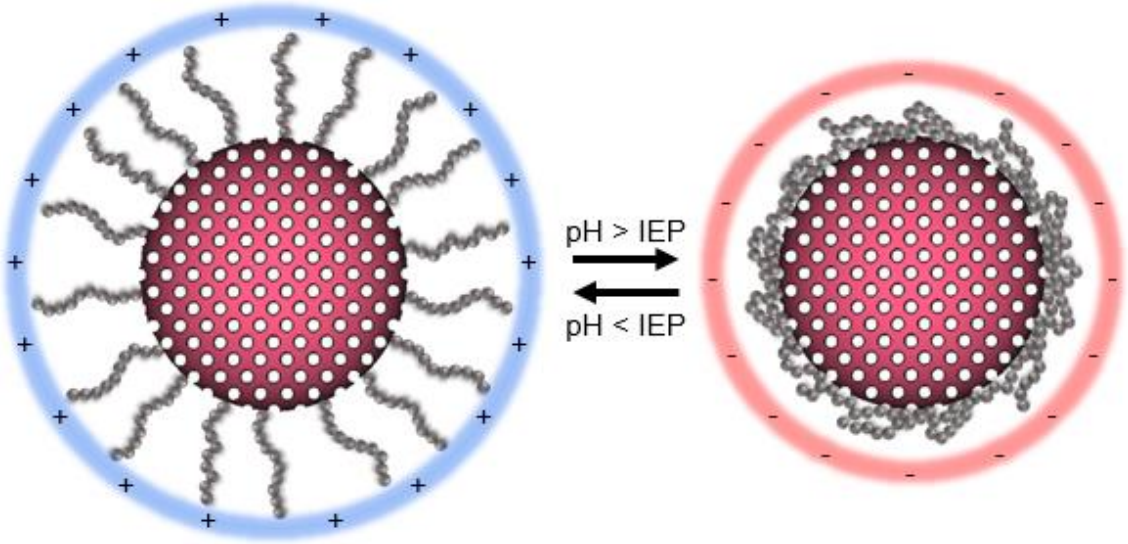

Figure 3.12. Electrokinetic charge expected for the hybrid systems at different pH values.

In figure 3.13 are shown the corresponding curves measured for the three samples obtained after each surface modification, MSN.APTES, MSN.RAFT and MSN.P(DPAEM) II b. As mentioned before on 3.2.3, the IEP of the amine group is 10.6 being fully protonated at lower values, so the presence of this group on silica surface should shift the IEP towards higher values than the obtained (pH 8). This could be due to the effect of free silanol groups present on the MSN surface not attached to the amine group (Rosenholm *et al.*, 2008). The shift of the MSN.RAFT curve to lower values confirm a successful RAFT immobilization as discussed on 3.2.3. Lastly, the homogenous covering of the MSN surface by RAFT polymerization was proven by the increment on ζ-Potential values, in comparison with MSN.RAFT. The IEP of the polymer attached to MSN can be estimated by analyzing the MSN.P(DPAEM) curve, being in between 6.2 and 6.5. These values are in agreement with the transmittance spectroscopy results for free polymer (see 3.3.3).

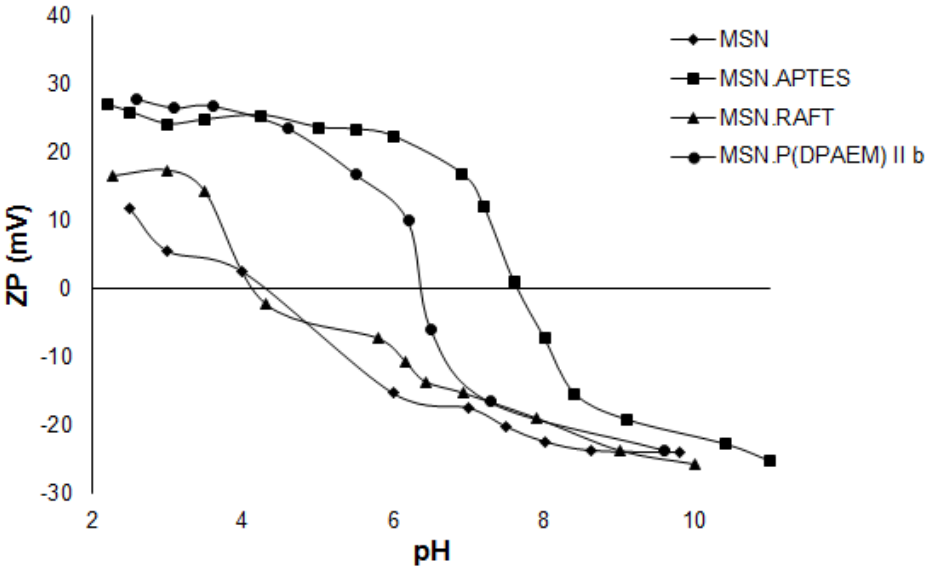

Figure 3.13. ζ-potential titrations for MSN (♦), MSN.APTES (■), MSN.RAFT(▲) and MSN.P(DPAEM) II b (●).

The corresponding ζ-Potential curves obtained for the sample before polymer graft, MSN.APTES, and after, MSN.G P(DPAEM) I are displayed in figure 3.14. A substantial difference between both curves is appreciated, suggesting a surface modification. However, the hybrid nanoparticle obtained by the *grafting to* approach does not show the same electrokinetic charge curve as the one obtained by *grafting from* (figure 3.12, MSN.P(DPAEM) II b). The shift to lower IEP value (~ 5) could be explained by low and non-homogenous polymeric shell covering, being the IEP value affected by free silanol groups from the MSNs surface. This effect is not significant on the electrical charge for the hybrid system obtained by the *grafting from*, supported by the similar pk_a obtained for the free polymer and the hybrid system. The low effectiveness of this process proven by ζ -potential are in agreement with the results obtained by ^1H NMR.

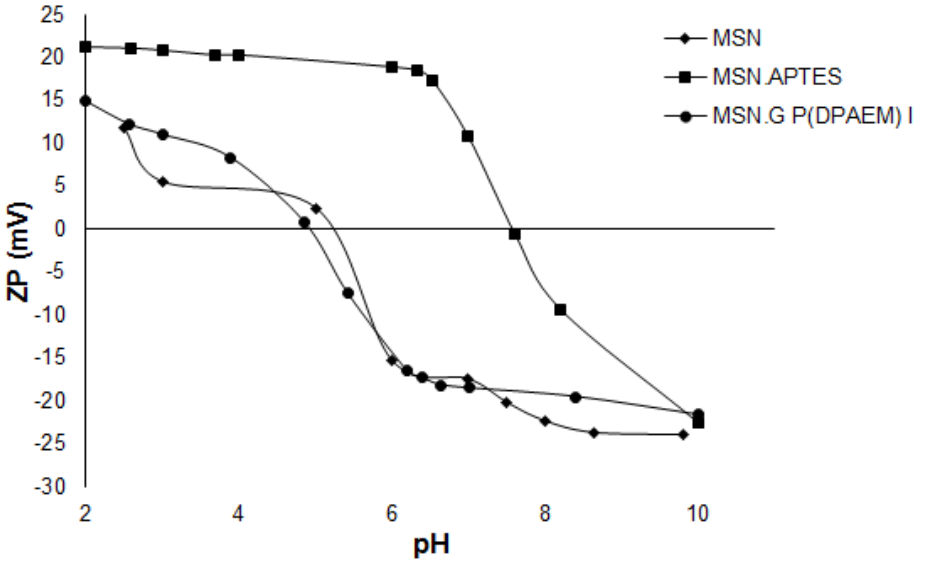

Figure 3.14. ζ-potential titrations for MSN (♦), MSN.APTES(■) and MSN.G P(DPAEM) I (●).

3.5. Cell Viability

To examine biocompatibility of the hybrid system we tested the cytotoxicity of the material in mammary carcinoma cell line MCF-7. The human mammary carcinoma cell line MCF-7 were grown as adherent culture and maintained routinely in DMEM containing 10 % FBS, and 1 % antibiotic solution containing penicillin and streptomycin at 37°C in 5 % CO_2. For the cell viability assay (MTT), cells were seeded onto the 96 well plates and incubated for 24 h prior to the experiments. The cytotoxic effect of the synthesized MSN.P(DPAEM) II b and MSN.G P(DPAEM) I was determined by MTT assay. This method is based on the change of color of yellow to purple when MTT is reduced in the mitochondria of living cells, so the conversion can be directly related to the number of viable (living) cells. The absorbance of this colored solution can be quantified using a spectrophotometer. Briefly, MCF-7 cells were plated at a density of 5×104 cells per well into the 96-well plate and cultured for 24 h at 37ºC. When the cells were about 70-80 % confluent, the synthesized NPs at different concentrations (0 - 125 µg/ml) were added in triplicates and incubated for 24 h. After the incubation period, media from each wells were carefully replaced with 100 µl of fresh complete media without disturbing the cells, followed by addition of 20 µl of MTT solution (5 mg/ml in PBS) to each well and incubated for 4 h at 37ºC. Finally, the formazan crystals formed in each well was dissolved using 150 µl of MTT solvent (4 mM HCl and 0.1 % NP40 in isopropanol) and the absorbance was read at 590 nm.

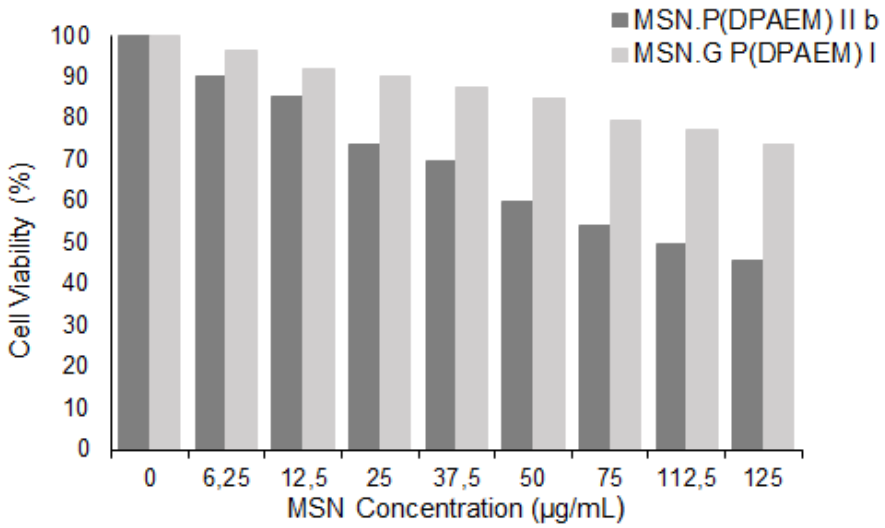

Figure 3.15. Cell viability obtained by MTT assay for MSN.P(DPAEM) II b (dark grey) and MSN.G P(DPAEM) I (light grey) with different concentrations during 24 h.

In figure 3.15 the cell viability as a function of the concentration of the hybrid system is shown. The results for MSN.G P(DPAEM) I show better biocompatibility than MSN.P(DPAEM) II b. The results for MSN.P(DPAEM) II b were unexpected, since as discuss before, this MSN have a homogeneous polymeric cover which would increase the biocompatibility of the system. A possible reason for this results would be the presence of solvent remaining in the MSN's pores and not being release during the wash process due to the efficiency of the polymeric coating.

4. Conclusion and Future Perspectives

The continuous effort to improve the effectiveness of the drugs and a decrease of their side effects originates the need to develop new systems able to carry the drug molecules to the target, avoiding its metabolization/degradation by the body and improving its selectivity. In this work, synthesis and characterization of a new hybrid system, based on a mesoporous silica nanoparticle (MSN) core and a pH-responsive polymeric shell, was performed.

MSN were synthesized with a fluorescent dye on its structure and were submitted to amine surface modification process using APTES. The APTES molecule served as an anchor for the CTA immobilization which allowed the 2 – (Diisopropylamino) ethyl methacrylate (DPAEM) monomer controlled polymerization from the MSN surface.

TEM and DLS characterization confirmed the success on the synthesis of spherical MSN with narrow polydispersity and a well-defined mesostructure was successfully obtained by the method used. Different NaOH concentrations yielded nanoparticles of different diameter.

Amine surface modification was assessed by ^{1}H NMR, obtaining 1.6 – 3.1 mmol per gram of MSN, and a successful CTA immobilization was verified by UV-Vis Spectroscopy with an estimated CTA surface concentration between 2.0 and 3.1 mmol per gram of MSN. Those surface modifications were confirmed by the variation on ζ-potential. The ζ-potential average for free MSN was -23.5 mV, 30.4 mV for MSN.APTES and -8.0 mV for MSN.RAFT.

2 – (Diisopropylamino) ethyl methacrylate (DPAEM) monomer and 2 – (Diisopropylamino) ethyl methacrylate polymer (P(DPAEM)) structures were determined by ^{1}H NMR. The yield of monomer synthesis was around 60 – 70 % and the estimated yield for DPAEM polymerization was 32.70 %. The pH responsive behaviour of P(DPAEM) was tested by UV-Vis Spectroscopy and through the transmittance titration the value of the pK_a could be estimated, being between 6.3 and 6.5.

The hybrid MSN were synthesized by the *grafting from* and the *grafting to* approaches, in order to compare the effectiveness of those processes. The average size obtained in milli-Q water pH (~ 5) for hybrid MSN by DLS was between 127 and 170 nm. In addition, TEM images suggest the presence of the polymeric shell. For greater confirmation, ^{1}H NMR, FT-IR Spectroscopy and Zeta -Potential techniques were used.

The ^{1}H NMR spectra obtained for the hybrid nanoparticles produced by *grafting from* approach suggests that the polymerization occurs, although it was not complete, proved by the presence of peaks attributed to the monomer structure, even after the washing process. On the other hand, the spectra of the hybrid nanoparticles produced by *grafting to* approach suggests a low polymer attachment on the MSN surface, due to the mostly free APTES molecule present on the sample and due to the low intensity of peaks associated with the polymer.

ζ-potential titration confirmed the presence of the homogeneous polymeric coating. The electrokinetic behaviour of the hybrid nanoparticles, with IEP for the hybrid MSN obtained by *grafting from* approach estimated by ζ-potential analysis between 6.2 and 6.5. The lowest IEP shown by the hybrid MSN obtained by *grafting to* approach can be related with a low and non-homogeneous polymeric coating, this event supported by ^{1}H NMR results.

FT-IR Spectroscopy was recorded for MSN.P(DPAEM) obtained by *grafting from* approach, proving APTES, CTA and polymer attachment to the MSN surface.

The goals of this work were successfully accomplished, since hybrid mesoporous silica nanoparticles, coated with a pH-responsive polymer synthesis and characterization was achieved. In addition, it was proved that *grafting from* approach is more effective than *grafting to* strategy even it is necessary to improve the washing process for those materials and verify the biocompatibility of the system.

For the characterization of the polymer obtained by RAFT polymerization, gel permeation chromatography (GPC) was performed, but the polymer adsorbed to the different columns tested.

Furthermore, the pH-responsive behavior could be better understood by a controlled release assay through fluorescence spectroscopy, by incorporating a fluorescent compound, such as sulforhodamine B (SRB), or even a fluorescent drug, as doxorubicin, into the hybrid system.

Once these assays are concluded, it should be of great interest to repeat viability assay and determine the internalization of this hybrid system, as well as to study the drug controlled release *in vitro* to confirm the advantage of using this platform as a future and promising strategy, compared to the conventional treatments applied until now. For those assays it would be of great interest to analyse the relation between nanoparticle size and the polymer length with its biocompatibility and its effectiveness of cargo host/release in order to develop an optimize system of great interest for medical applications.

5. References

Ahmadi, E., Dehghannejad, N., Hashemikia, S., Ghasemnejad, M., & Tabebordbar, H. 2014. Synthesis and surface modification of mesoporous silica nanoparticles and its application as carriers for sustained drug delivery. *Drug delivery*, *21*(3), 164-172.

Argyo, C., Weiss, V., Bräuchle, C., & Bein, T. 2013. Multifunctional mesoporous silica nanoparticles as a universal platform for drug delivery. *Chemistry of Materials*, *26*(1), 435-451.

Bawa, P., Pillay, V., Choonara, Y. E., & Du Toit, L. C. 2009. Stimuli-responsive polymers and their applications in drug delivery. *Biomedical materials*, *4*(2), 022001.

Beck, J. S., Vartuli, J. C., Roth, W. J., Leonowicz, M. E., Kresge, C. T., Schmitt, K. D., Chu, C. T. W., Olson, D. H., Sheppard, E. W., McCullen, S. B., Higgins, J. B., & Schlenker, J. L. 1992. A new family of mesoporous molecular sieves prepared with liquid crystal templates. *Journal of the American Chemical Society*, *114*(27), 10834-10843.

Bhattacharjee, S. 2016. DLS and zeta potential–What they are and what they are not?. *Journal of Controlled Release.*

Cabane, E., Zhang, X., Langowska, K., Palivan, C. G., & Meier, W. 2012. Stimuli-responsive polymers and their applications in nanomedicine. *Biointerphases*, *7*(1), 9.

Chaudhuri, R., & Paria, S. 2011. Core/shell nanoparticles: classes, properties, synthesis mechanisms, characterization, and applications. *Chemical reviews*, *112*(4), 2373-2433.

Crucho, C. I. C., Baleizão, C. M., Farinha, J. P. 2016. Functional group coverage and conversion quantification in nanostructured silica by 1H-NMR. *Analytical Chemistry*.

Cuenca, A. G., Jiang, H., Hochwald, S. N., Delano, M., Cance, W. G., & Grobmyer, S. R. 2006. Emerging implications of nanotechnology on cancer diagnostics and therapeutics. *Cancer*, *107*(3), 459-466.

Cunningham, A., & Bürgi, T. 2013. Bottom-up Organisation of Metallic Nanoparticles. Springer Berlin Heidelberg. *Amorphous Nanophotonics,* 1-37.

Dai, S., Ravi, P., & Tam, K. C. 2008. pH-Responsive polymers: synthesis, properties and applications. *Soft Matter*, *4*(3), 435-449.

De Barros, A. L. B., de Oliveira Ferraz, K. S., Dantas, T. C. S., Andrade, G. F., Cardoso, V. N., & de Sousa, E. M. B. 2015. Synthesis, characterization, and biodistribution studies of 99m Tc-labelled SBA-16 mesoporous silica nanoparticles. *Materials Science and Engineering: C*, *56*, 181-188.

DeMuth, P., Hurley, M., Wu, C., Galanie, S., Zachariah, M. R., & DeShong, P. 2011. Mesoscale porous silica as drug delivery vehicles: Synthesis, characterization, and pH-sensitive release profiles. *Microporous and Mesoporous Materials*, *141*(1), 128-134.

Faccia, P. A., & Amalvy, J. I. 2013. Synthesis, characterization, and swelling behavior of new pH-sensitive hydrogels derived from copolymers of 2-hydroxyethyl methacrylate and 2-(diisopropylamino)ethyl methacrylate. *Journal of Applied Polymer Science*, *127*(3), 1974-1980.

Favier, A., & Charreyre, M. T. 2006. Experimental Requirements for an Efficient Control of Free-Radical Polymerizations via the Reversible Addition-Fragmentation Chain Transfer (RAFT) Process. *Macromolecular Rapid Communications*, *27*(9), 653-692.

Ferrari, M. 2005. Cancer nanotechnology: opportunities and challenges. *Nature Reviews Cancer*, *5*(3), 161-171.

Feynman, R. P. December 29th 1959. There's plenty of room at the bottom. *The Vega Science Trust*. The American Physical Society at CalTech, California.

Gao, X., Kucerka, N., Nieh, M. P., Katsaras, J., Zhu, S., Brash, J. L., & Sheardown, H. 2009. Chain conformation of a new class of PEG-based thermoresponsive polymer brushes grafted on silicon as determined by neutron reflectometry. *Langmuir*, *25*(17), 10271-10278.

Gaynor, S., Greszta, D., Mardare, D., Teodorescu, M., & Matyjaszewski, K. 1994. Controlled radical polymerization. *Journal of Macromolecular Science, Part A*, *31*(11), 1561-1578.

Gil, E. S., & Hudson, S. M. 2004. Stimuli-reponsive polymers and their bioconjugates. *Progress in polymer science*, *29*(12), 1173-1222.

Góis, J. R., Rocha, N., Popov, A. V., Guliashvili, T., Matyjaszewski, K., Serra, A. C., & Coelho, J. F. 2014. Synthesis of well-defined functionalized poly (2-(diisopropylamino) ethyl methacrylate) using ATRP with sodium dithionite as a SARA agent. *Polymer Chemistry*, *5*(12), 3919-3928.

Goodsell, D. S. 2004. Bionanotechnology: lessons from nature. *Willey-Less, 311*, 1-8.

Green, D. L., Jayasundara, S., Lam, Y. F., & Harris, M. T. 2003. Chemical reaction kinetics leading to the first Stober silica nanoparticles–NMR and SAXS investigation. *Journal of non-crystalline solids*, *315*(1), 166-179.

Grün, M., Büchel, G., Kumar, D., Schumacher, K., Bidlingmaier, B., & Unger, K. K. 2000. Rational design, tailored synthesis and characterisation of ordered mesoporous silica in the micron and submicron size range. *Studies in surface science and catalysis*, *128*, 155-165.

Gupta, P., Vermani, K., & Garg, S. 2002. Hydrogels: from controlled release to pH-responsive drug delivery. *Drug discovery today*, *7*(10), 569-579.

Hench, L. L., & West, J. K. 1990. The sol-gel process. *Chemical Reviews*,*90*(1), 33-72.

Hu, Y. Q., Kim, M. S., Kim, B. S., & Lee, D. S. 2007. Synthesis and pH-dependent micellization of 2-(diisopropylamino) ethyl methacrylate based amphiphilic diblock copolymers via RAFT polymerization. *Polymer*, *48*(12), 3437-3443.

Huang, X., Appelhans, D., Formanek, P., Simon, F., & Voit, B. 2011. Synthesis of well-defined photo-cross-linked polymeric nanocapsules by surface-initiated RAFT polymerization. *Macromolecules*, *44*(21), 8351-8360.

Huh, K. M., Kang, H. C., Lee, Y. J., & Bae, Y. H. 2012. pH-sensitive polymers for drug delivery. *Macromolecular research*, *20*(3), 224-233.

Huh, S., Wiench, J. W., Yoo, J. C., Pruski, M., & Lin, V. S. Y. 2003. Organic functionalization and morphology control of mesoporous silicas via a co-condensation synthesis method. *Chemistry of materials*, *15*(22), 4247-4256.

Jain, K. K. 2005. Nanotechnology-based drug delivery for cancer. *Technology in cancer research & treatment*, *4*(4), 407-416.

Kim, S., Kim, J. H., Jeon, O., Kwon, I. C., & Park, K. 2009. Engineered polymers for advanced drug delivery. *European Journal of Pharmaceutics and Biopharmaceutics*, *71*(3), 420-430.

Li, Z., Barnes, J. C., Bosoy, A., Stoddart, J. F., & Zink, J. I. 2012. Mesoporous silica nanoparticles in biomedical applications. *Chemical Society Reviews*, *41*(7), 2590-2605.

Liu, C., Guo, J., Yang, W., Hu, J., Wang, C., & Fu, S. 2009. Magnetic mesoporous silica microspheres with thermo-sensitive polymer shell for controlled drug release. *Journal of Materials Chemistry*, *19*(27), 4764-4770.

Ma, M., Zheng, S., Chen, H., Yao, M., Zhang, K., Jia, X., Mou, J., Xu, H., Wu, R., & Shi, J. 2014. A combined “RAFT” and “Graft From” polymerization strategy for surface modification of mesoporous silica nanoparticles: towards enhanced tumor accumulation and cancer therapy efficacy. *Journal of Materials Chemistry B*,*2*(35), 5828-5836.

Matyjaszewski, K. 1996. Controlled radical polymerization. *Current Opinion in Solid State and Materials Science*, *1*(6), 769-776.

Moad, G., Rizzardo, E., & Thang, S. H. 1998. Living free-radical polymerization by reversible addition-fragmentation chain transfer: the RAFT process. *Macromolecules*, *31*(16), 5559-5562.

Moad, G., Rizzardo, E., & Thang, S. H. 2005. Living radical polymerization by the RAFT process. *Australian journal of chemistry*, *58*(6), 379-410.

Mousa, S. A., & Bharali, D. J. 2011. Nanotechnology-based detection and targeted therapy in cancer: nano-bio paradigms and applications. *Cancers*, *3*(3), 2888-2903.

Natarajan, S. K., & Selvaraj, S. 2014. Mesoporous silica nanoparticles: importance of surface modifications and its role in drug delivery. *Rsc Advances*, *4*(28), 14328-14334.

National Nanotechnology Initiative (NNI). 2014. What is nanotechnology? Available online: http://www.nano.gov/nanotech-101/what/definition (accessed on 12th October 2015).

Odian, G. 2004. Radical chain polymerization. Principles of polymerization. *John Wiley & Sons, 4, 198-349*.

Peng, C. L., Yang, L. Y., Luo, T. Y., Lai, P. S., Yang, S. J., Lin, W. J., & Shieh, M. J. 2010. Development of pH sensitive 2-(diisopropylamino) ethyl methacrylate based nanoparticles for photodynamic therapy. *Nanotechnology*,*21*(15), 155103.

Popat, A., Hartono, S. B., Stahr, F., Liu, J., Qiao, S. Z., & Lu, G. Q. M. 2011. Mesoporous silica nanoparticles for bioadsorption, enzyme immobilisation, and delivery carriers. *Nanoscale*, *3*(7), 2801-2818.

Ribeiro, T., Raja, S., Rodrigues, A. S., Fernandes, F., Farinha, J. P. S., & Baleizão, C. 2013. High performance NIR fluorescent silica nanoparticles for bioimaging. *RSC Advances*, *3*(24), 9171-9174.

Rodrigues, A. S., Ribeiro, T., Fernandes, F., Farinha, J. P. S., & Baleizão, C. 2013. Intrinsically fluorescent silica nanocontainers: a promising theranostic platform. *Microscopy and Microanalysis*, *19*(05), 1216-1221.

Rosenholm, J. M., & Lindén, M. 2008. Towards establishing structure–activity relationships for mesoporous silica in drug delivery applications. *Journal of controlled release*, *128*(2), 157-164.

Ross, J., Schreiber, I., & Vlad, M. O. 2005. Determination of complex reaction mechanisms: analysis of chemical, biological, and genetic networks. *Oxford University Press*.

Santiago, A. M., Ribeiro, T., Rodrigues, A. S., Ribeiro, B., Frade, R. F., Baleizão, C., & Farinha, J. P. S. 2015. Multifunctional Hybrid Silica Nanoparticles with a Fluorescent Core and Active Targeting Shell for Fluorescence Imaging Biodiagnostic Applications. *European Journal of Inorganic Chemistry*, *2015*(27), 4579-4587.

Schmaljohann, D. 2006. Thermo-and pH-responsive polymers in drug delivery. *Advanced drug delivery reviews*, *58*(15), 1655-1670.

Schulz, A., & McDonagh, C. 2012. Intracellular sensing and cell diagnostics using fluorescent silica nanoparticles. *Soft Matter*, *8*(9), 2579-2585.

Singh, N., Karambelkar, A., Gu, L., Lin, K., Miller, J. S., Chen, C. S., Sailor, M. J., & Bhatia, S. N. 2011. Bioresponsive mesoporous silica nanoparticles for triggered drug release. *Journal of the American Chemical Society*, *133*(49), 19582-19585.

Singh, S. 2010. Nanomedicine–nanoscale drugs and delivery systems. *Journal of nanoscience and nanotechnology*, *10*(12), 7906-7918.

Slowing, I., Trewyn, B. G., & Lin, V. S. Y. 2006. Effect of surface functionalization of MCM-41-type mesoporous silica nanoparticles on the endocytosis by human cancer cells. *Journal of the American Chemical Society*, *128*(46), 14792-14793.

Slowing, I., Vivero-Escoto, J. L., Trewyn, B. G., & Lin, V. S. Y. 2010. Mesoporous silica nanoparticles: structural design and applications. *Journal of Materials Chemistry*, *20*(37), 7924-7937.

Soler-Illia, G. J., & Azzaroni, O. 2011. Multifunctional hybrids by combining ordered mesoporous materials and macromolecular building blocks. *Chemical Society Reviews*, *40*(2), 1107-1150.

Stein, A., Melde, B. J., & Schroden, R. C. 2000. Hybrid inorganic–organic mesoporous silicates—nanoscopic reactors coming of age. *Advanced Materials*, *12*(19), 1403-1419.

Stenzel, M. H., Davis, T. P., & Fane, A. G. 2003. Honeycomb structured porous films prepared from carbohydrate based polymers synthesized via the RAFT process. *Journal of Materials Chemistry*, *13*(9), 2090-2097.

Stöber, W., Fink, A., & Bohn, E. 1968. Controlled growth of monodisperse silica spheres in the micron size range. *Journal of colloid and interface science*, *26*(1), 62-69.

Storhoff, J. J., Mucic, R. C., & Mirkin, C. A. 1997. Strategies for organizing nanoparticles into aggregate structures and functional materials. *Journal of Cluster Science*, *8*(2), 179-216.

Strebhardt, K., & Ullrich, A. 2008. Paul Ehrlich's magic bullet concept: 100 years of progress. *Nature Reviews Cancer*, *8*(6), 473-480.

Tan, W., Wang, K., He, X., Zhao, X. J., Drake, T., Wang, L., & Bagwe, R. P. 2004. Bionanotechnology based on silica nanoparticles. *Medicinal research reviews*, *24*(5), 621-638.

Tang, F., Li, L., & Chen, D. 2012. Mesoporous silica nanoparticles: synthesis, biocompatibility and drug delivery. *Advanced Materials*, *24*(12), 1504-1534.

Trewyn, B. G., Slowing, I. I., Giri, S., Chen, H. T., & Lin, V. S. Y. 2007. Synthesis and functionalization of a mesoporous silica nanoparticle based on the sol–gel process and applications in controlled release. *Accounts of Chemical Research*, *40*(9), 846-853.

Vallet-Regí, M. 2012. Mesoporous silica nanoparticles: their projection in nanomedicine. *ISRN Materials Science.*

Vega-Rios, A., & Licea-Claveríe, A. 2011. Controlled synthesis of block copolymers containing N-isopropylacrylamide by reversible addition-fragmentation chain-transfer (RAFT) polymerization. *Journal of the Mexican Chemical Society*, *55*(1), 21-32.

Wang, Y., Han, N., Zhao, Q., Bai, L., Li, J., Jiang, T., & Wang, S. 2015. Redox-responsive mesoporous silica as carriers for controlled drug delivery: a comparative study based on silica and PEG gatekeepers. *European Journal of Pharmaceutical Sciences*, *72*, 12-20.

Xu, R. 2008. Progress in nanoparticles characterization: Sizing and zeta potential measurement. *Particuology*, *6*(2), 112-115.

Zhang, Q., Neoh, K. G., Xu, L., Lu, S., Kang, E. T., Mahendran, R., & Chiong, E. 2014. Functionalized mesoporous silica nanoparticles with mucoadhesive and sustained drug release properties for potential bladder cancer therapy.*Langmuir*, *30*(21), 6151-6161.

Zhao, Y., Trewyn, B. G., Slowing, I. I., & Lin, V. S. Y. 2009. Mesoporous silica nanoparticle-based double drug delivery system for glucose-responsive controlled release of insulin and cyclic AMP. *Journal of the American Chemical Society*, *131*(24), 8398-8400.

Zhu, J., *et al.* 2013. Size-dependent cellular uptake efficiency, mechanism, and cytotoxicity of silica nanoparticles toward HeLa cells. *Talanta*, *107*, 408-415.

Zou, H., Wu, S., & Shen, J. 2008. Polymer/silica nanocomposites: preparation, characterization, properties, and applications. *Chem. Rev*, *108*(9), 3893-3957.

Appendix A

Example of DLS result obtained for MSN D.P(DPAEM) I, MSN E.P(DPAEM) II a and MSN E.P(DPAEM) II b. All of these results meets quality criteria.

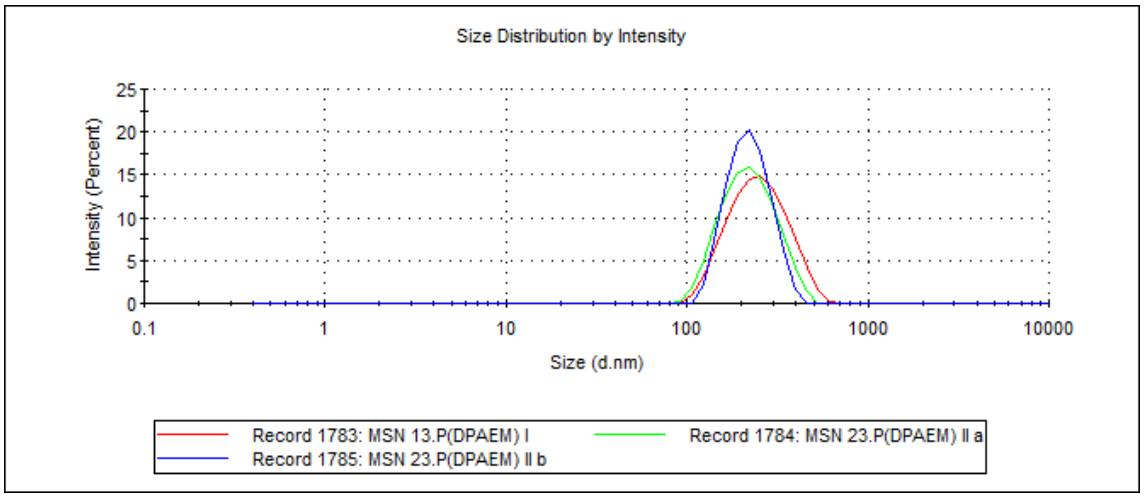

Figure a.1. Size distribution by intensity obtained by DLS for MSN D.P(DPAEM) I (red), MSN E.P(DPAEM) II a (green) and MSN E.P(DPAEM) II b (blue).

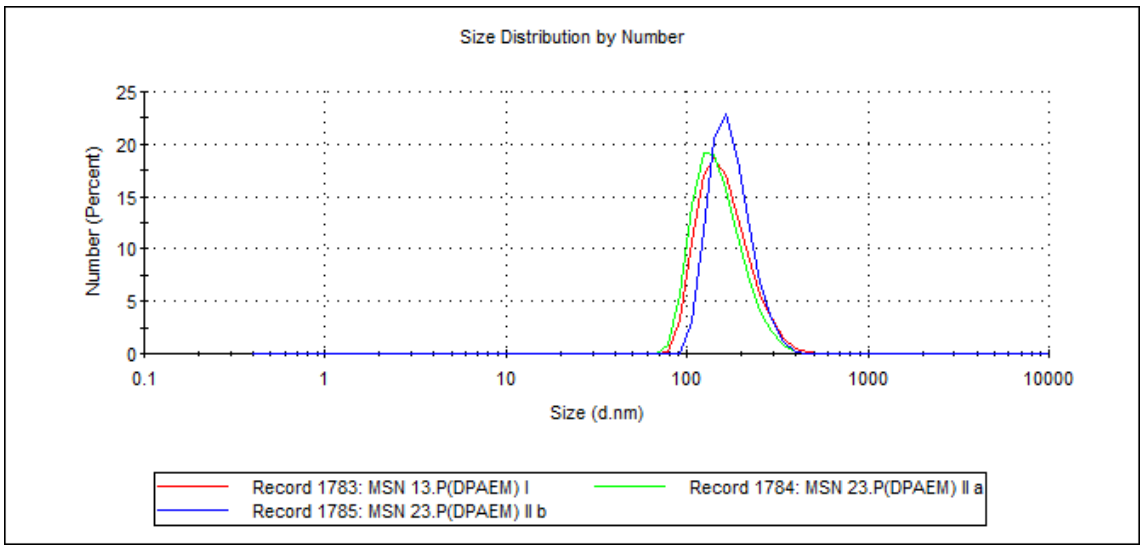

Figure a.2. Size distribution by number obtained by DLS for MSN D.P(DPAEM) I (red), MSN E.P(DPAEM) II a (green) and MSN E.P(DPAEM) II b (blue).

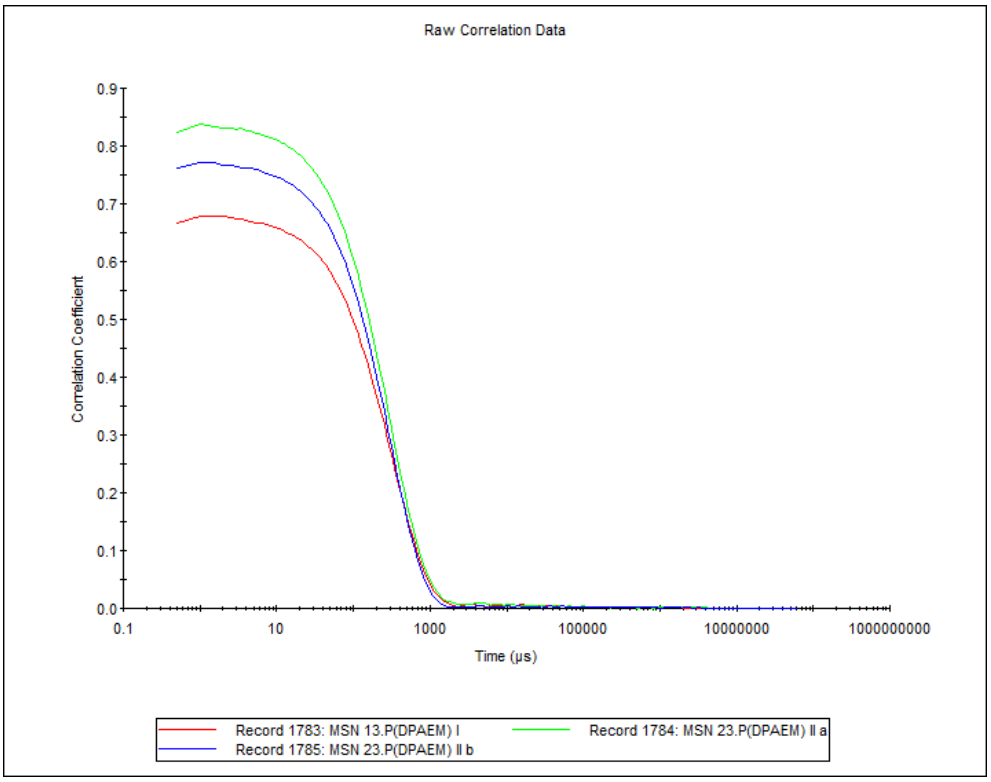

Figure a.3. Correlogram obtained by DLS for MSN D.P(DPAEM) I (red), MSN E.P(DPAEM) II a (green) and MSN E.P(DPAEM) II b (blue).

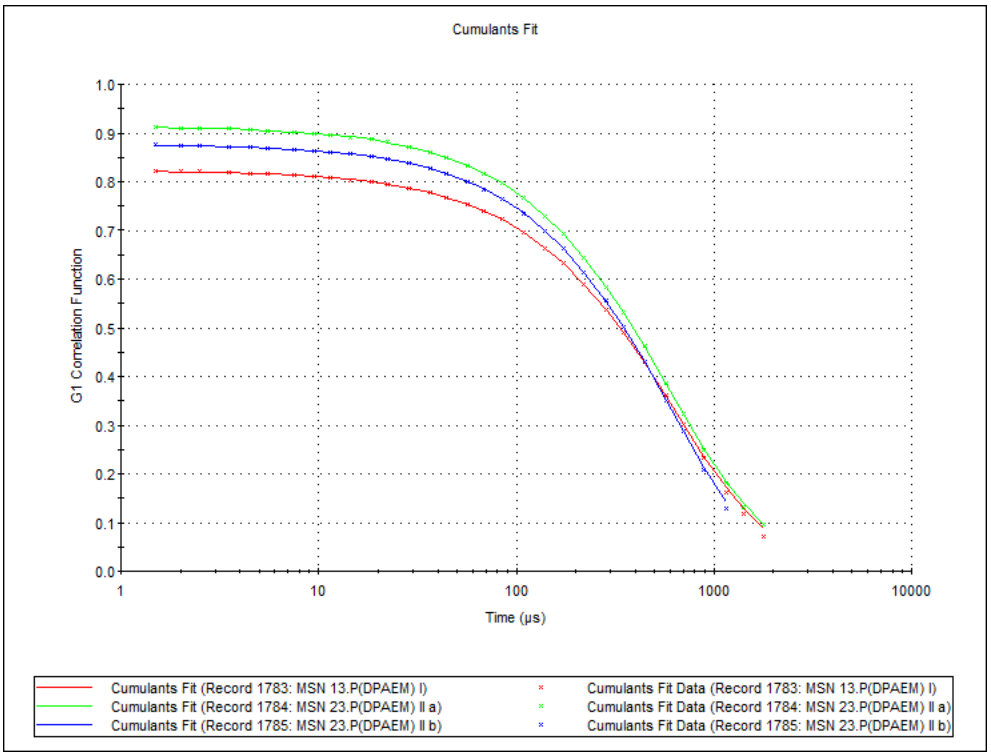

Figure a.3. Cumulants fit obtained by DLS for MSN D.P(DPAEM) I (red), MSN E.P(DPAEM) II a (green) and MSN E.P(DPAEM) II b (blue).

b

Appendix B

Example of DLS result obtained for MSN E.P(DPAEM) III a and MSN E.P(DPAEM) III b, MSN D.G P(DPAEM) I, MSN F.G P(DPAEM) I and MSN E.P(DPAEM) II a at pH 3. All of these results do not meet quality criteria.

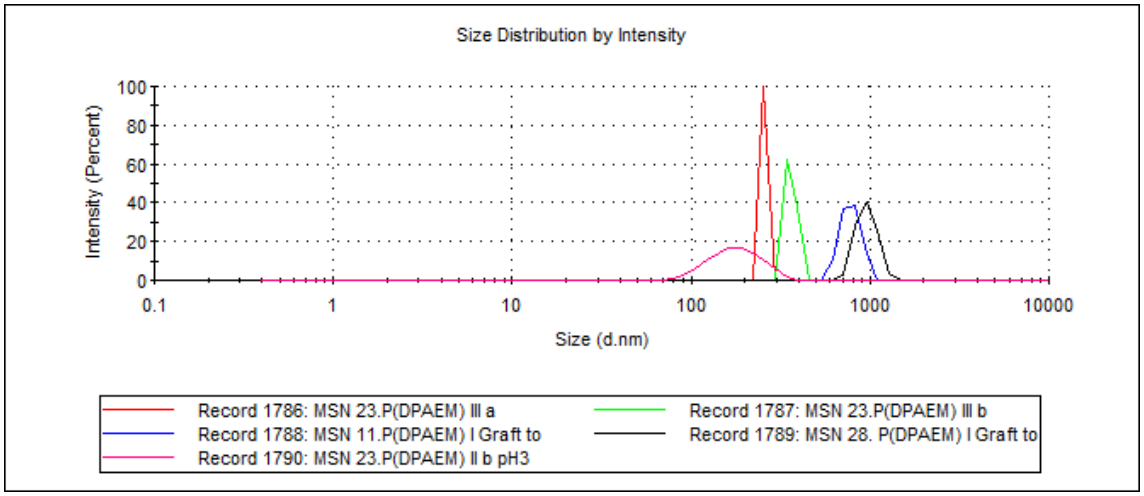

Figure b.1. Size distribution by intensity obtained by DLS for MSN E.P(DPAEM) III a (red) and MSN E.P(DPAEM) III b (green), MSN C.G P(DPAEM) I (blue), MSN F.G P(DPAEM) I (black) and MSN E.P(DPAEM) III a (pink).

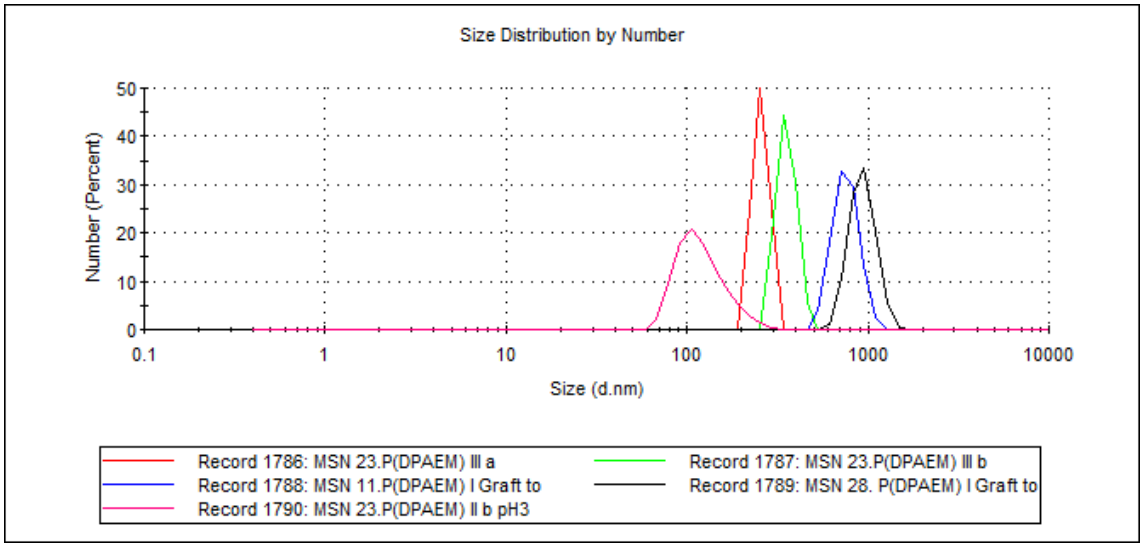

Figure b.2. Size distribution by number obtained by DLS for MSN E.P(DPAEM) III a (red) and MSN E.P(DPAEM) III b (green), MSN C.G P(DPAEM) I (blue), MSN F.G P(DPAEM) I (black) and MSN E.P(DPAEM) III a (pink).

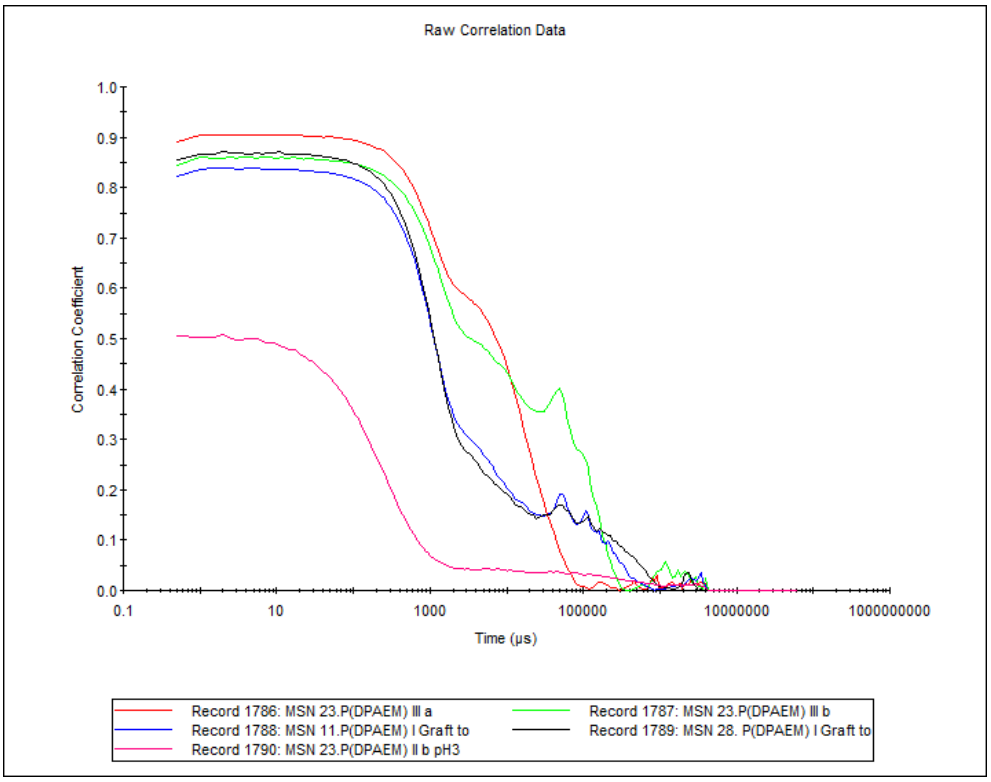

Figure b.3. Correlogram obtained by DLS for MSN E.P(DPAEM) III a (red) and MSN E.P(DPAEM) III b (green), MSN C.G P(DPAEM) I (blue), MSN F.G P(DPAEM) I (black) and MSN E.P(DPAEM) III a (pink).

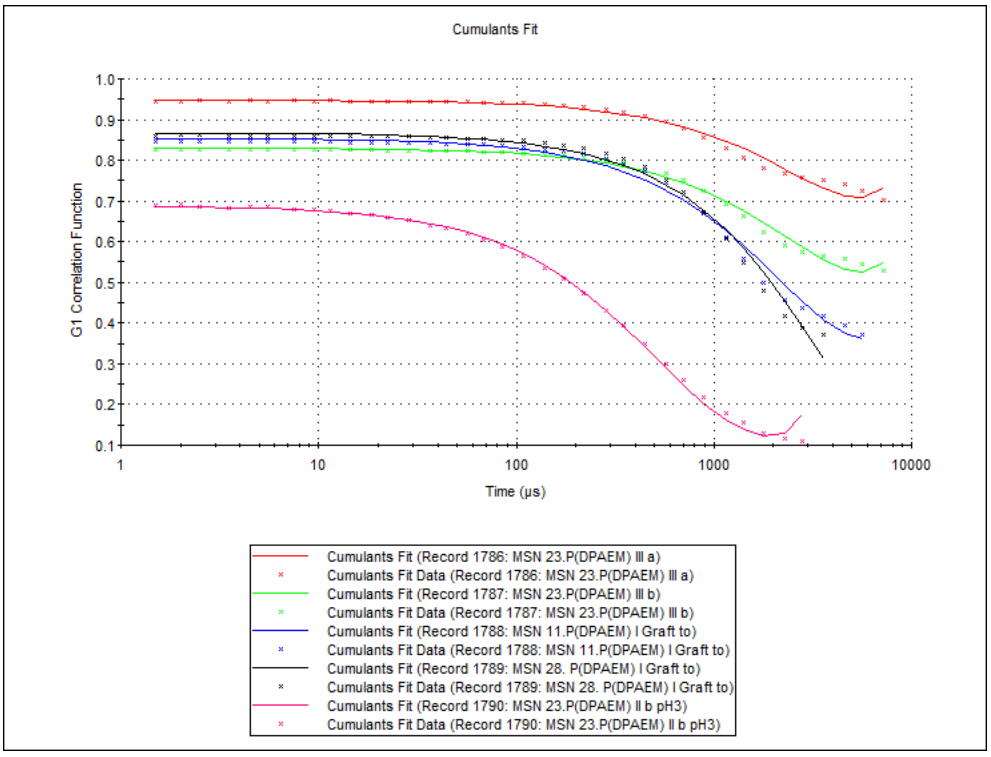

Figure b.4. Cumlants fit obtained by DLS for MSN E.P(DPAEM) III a (red) and MSN E.P(DPAEM) III b (green), MSN C.G P(DPAEM) I (blue), MSN F.G P(DPAEM) I (black) and MSN E.P(DPAEM) III a (pink).